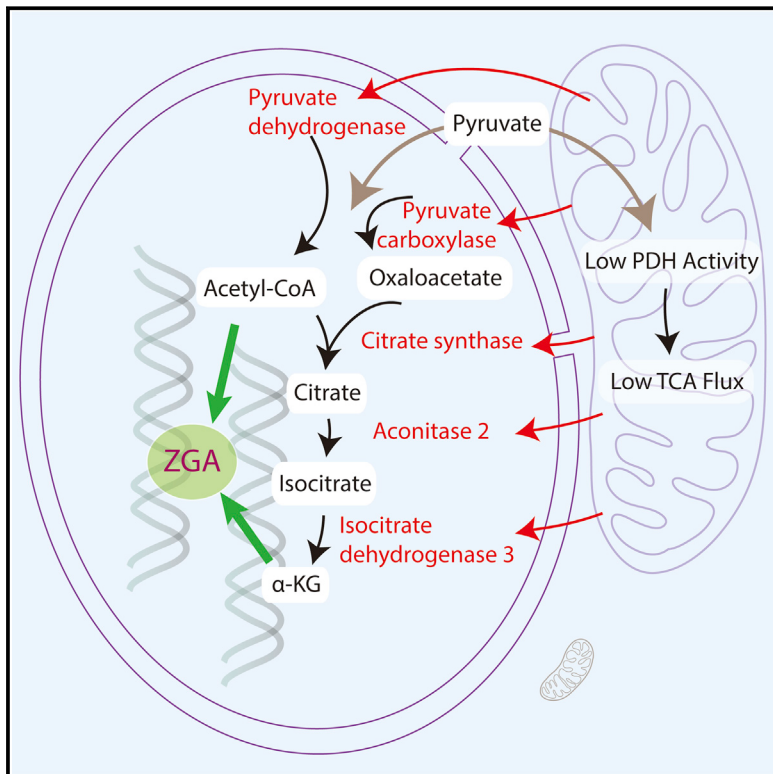


Nuclear Localization of Mitochondrial TCA Cycle Enzymes as a Critical Step in Mammalian Zygotic Genome Activation

Graphical Abstract



Authors

Raghavendra Nagaraj, Mark S. Sharpley, Fangtao Chi, ..., Rachel Kim, Amander T. Clark, Utpal Banerjee

Correspondence

banerjee@mbi.ucla.edu

In Brief

Mitochondrial enzymes in the nucleus synthesize metabolites for epigenetic remodeling during zygote activation.

Highlights

- A subclass of active mitochondrial TCA cycle enzymes transiently moves to the nucleus
- Nuclear TCA proteins and metabolites are essential for zygotic genome activation (ZGA)
- Pyruvate, O-glycosylation, and chaperones are essential for this nuclear localization
- In both human and mouse embryos, PDH is nuclear when ZGA occurs in these species

Nuclear Localization of Mitochondrial TCA Cycle Enzymes as a Critical Step in Mammalian Zygotic Genome Activation

Raghavendra Nagaraj,^{1,6} Mark S. Sharpley,^{1,6} Fangtao Chi,¹ Daniel Braas,⁵ Yonggang Zhou,¹ Rachel Kim,¹ Amander T. Clark,^{1,2,4} and Utpal Banerjee^{1,2,3,4,7,*}

¹Department of Molecular, Cell and Developmental Biology

²Molecular Biology Institute

³Department of Biological Chemistry

⁴Eli and Edythe Broad Center of Regenerative Medicine and Stem Cell Research

⁵UCLA Center for Metabolomics

University of California, Los Angeles, Los Angeles, CA 90095, USA

⁶Co-first author

⁷Lead Contact

*Correspondence: banerjee@mbi.ucla.edu

<http://dx.doi.org/10.1016/j.cell.2016.12.026>

SUMMARY

Transcriptional control requires epigenetic changes directed by mitochondrial tricarboxylic acid (TCA) cycle metabolites. In the mouse embryo, global epigenetic changes occur during zygotic genome activation (ZGA) at the 2-cell stage. Pyruvate is essential for development beyond this stage, which is at odds with the low activity of mitochondria in this period. We now show that a number of enzymatically active mitochondrial enzymes associated with the TCA cycle are essential for epigenetic remodeling and are transiently and partially localized to the nucleus. Pyruvate is essential for this nuclear localization, and a failure of TCA cycle enzymes to enter the nucleus correlates with loss of specific histone modifications and a block in ZGA. At later stages, however, these enzymes are exclusively mitochondrial. In humans, the enzyme pyruvate dehydrogenase is transiently nuclear at the 4/8-cell stage coincident with timing of human embryonic genome activation, suggesting a conserved metabolic control mechanism underlying early pre-implantation development.

INTRODUCTION

Mammalian pre-implantation development initiates with the release of oocytes from the ovary, followed by fertilization resulting in a single-cell zygote. In mouse, the zygote undergoes three to four rounds of cell division, compacting at the 8-cell stage and then gives rise to a morula. The first differentiation step results in a blastocyst containing an inner cell mass (ICM) of cells, progenitors to the embryo proper and a surrounding lining of trophectoderm (TE) cells that will form extra-embryonic tissues. Preimplantation development takes approximately 4 days in mice and 6 days in humans, and the blastocyst then implants

into the uterine wall (Cockburn and Rossant, 2010; Li et al., 2010). The preimplantation embryo derives and exchanges nutrients with the oviductal fluid, while the post-implantation embryo is vascularized and is exposed to the considerably larger repertoire of nutrients and growth factors from the maternal blood supply. This developmental program is recapitulated *ex vivo* when the zygote is grown in a defined medium (potassium-supplemented simplex optimized medium [KSOM]), most of whose components are present in the oviductal fluid (Lawitts and Biggers, 1991). Such cultured embryos can be transplanted to produce normal progeny in diverse mammalian species (McLaren and Biggers, 1958).

Several critical cellular events occur during the 1-cell and 2-cell stages of mouse pre-implantation development. By the end of the 2-cell stage, maternal endowments of most RNAs and some proteins are depleted, and development beyond this point requires the productive activation of the embryonic genome (Li et al., 2010). Major zygotic/embryonic genome activation (ZGA/EGA) takes place at the 2-cell stage in mouse (Aoki et al., 1997) and EGA in humans, occurs during the 4- to 8-cell stage (Niakan and Eggan, 2013). As expected, these processes are dependent on many structural and epigenetic changes to the maternal and the paternal genomes that are reprogrammed for the purpose of the embryo (Weaver et al., 2009). Such major reprogramming of the genome requires metabolites such as α -ketoglutarate (α -KG), essential for protein and DNA demethylation, acetyl-CoA required for protein acetylation, ATP for phosphorylation of substrates, and UDP-GlcNAc for glycosylation (Hardivillé and Hart, 2014; Martinez-Pastor et al., 2013), production of each is dependent on the mitochondrial enzymes driving the tri-carboxylic acid (TCA) cycle and the utilization of pyruvate by pyruvate dehydrogenase. However, analysis of the early cleavage stages shows that the embryo has low metabolic activity (Leese, 2012) compared with the metabolic activity in the blastocyst or in adult tissues (Brinster, 1967a). The mitochondria appear small and rounded, lacking cristae at the 1- to 2-cell stages but are well formed in later stages (Calarco and Brown, 1969). Measurements of glucose metabolism (Brinster, 1967b;

Lane and Gardner, 2000; Leese and Barton, 1984) have shown that glucose consumption in cleavage-stage pre-implantation embryos is often more than 10-fold lower than in blastocysts. Metabolic processes such as the TCA cycle are coupled to the overall energetics of the cell and are therefore also attenuated (Barbehenn et al., 1978; Houghton et al., 1996). Similarly, the fate of metabolites consumed by the embryos is unusual. For example, only a fraction of pyruvate is completely oxidized in the mitochondria or reduced to lactate by lactate dehydrogenase (Lane and Gardner, 2000).

Both lactate and pyruvate are present in the oviductal fluid and are included in similar proportions in the ex vivo growth medium. Zygotes fail to survive in medium lacking both lactate and pyruvate. However, if only pyruvate is left out of the growth medium, the embryo is viable but fails to develop beyond the 2-cell stage (Brown and Whittingham, 1991). Under these conditions, lactate is not efficiently utilized because of the low NAD⁺/NADH ratio in the 2-cell embryo. Glucose is not substantially oxidized until the morula stage, and added glucose cannot be converted to pyruvate (Barbehenn et al., 1978; Brinster, 1969). However glucose is also included in the growth medium to support the entire pre-implantation developmental program from 1-cell to blastocyst, in serum-free conditions (Biggers et al., 1967; Leese, 2012; Brown and Whittingham, 1991). Embryos develop normally without requiring the import of proteins and amino acids from the medium, and, astonishingly, the 1-cell and 2-cell embryos complete their entire homeostatic processes even though amino acid accumulation, mitochondrial oxygen consumption, and glucose oxidation are all at very low levels (Brinster, 1969; Houghton et al., 1996). Low metabolic activity at early stages is thought to keep ROS levels low, thus avoiding DNA damage at a totipotent stage (Baumann et al., 2007).

In this paper, we demonstrate that a subset of mitochondrial enzymes of the TCA cycle briefly localize to and are active within the nucleus of the early stage embryo and are essential for the production of key metabolites that play a role in epigenetic remodeling during zygotic genome activation and developmental progression beyond the 2-cell stage.

RESULTS

Pyruvate Requirement in Early Stages of Embryogenesis

The first step in this study was to optimize the conditions of growth in a medium that is devoid of all amino acids or proteins and yet capable of sustaining pre-implantation development. Since the standard KSOM medium contains both, we developed a modified medium (mKSOM) (STAR Methods) that only contains the metabolites lactate, glucose and pyruvate, plus salts/buffer, and poly vinyl alcohol (Lawitts and Biggers, 1991). Zygotes are isolated 18 hr posthCG injection (STAR Methods) and cultured either in mKSOM medium that contains pyruvate (called +P medium for simplicity) or in mKSOM lacking pyruvate (or -P medium). Embryos grown in +P medium transition at the proper rate to the blastocyst stage (Figures 1A–1D), while those grown in -P medium are arrested at the 2-cell stage (Figures 1E–1H). A subset of embryos is blocked at the 1-cell stage in -P. These results are consistent with earlier studies that have used slightly

different media (Biggers et al., 1967; Brown and Whittingham, 1991). By switching the medium between +P and -P at various time points (Figure S1), the critical period for the pyruvate requirement is mapped to a 30-hr window between 24 and 54 hr (Figures 1I–1K'). At times outside this window, lactate substitutes pyruvate for normal development. All timings reported as hours in this paper are hours post-hCG (Figure 1I).

Bromodeoxyuridine (BrdU) incorporation and proliferating cell nuclear antigen (PCNA) expression, marking the S phase of the 2-cell stage, remain unchanged between embryos grown in +P or -P media (Figures 1L–1O). phospho-Histone3 (PH3) is first detected at very low levels at 45 hr in both +P and -P media (Figures 1P and 1Q). However, at 54 hr, late G2 phase, PH3 staining rises dramatically in +P but not in -P cultured embryos (Figures 1R and 1S). Consequently, pyruvate-deprived 2-cell embryos do not enter M phase, characterized by spindle assembly (Figures 1T and 1U).

Pyruvate Requirement in ZGA

In mouse embryos, ZGA initiates during the G2 phase of the 2-cell embryo (Aoki et al., 1997). As this is precisely the stage when the embryos arrest in the absence of pyruvate, we used several different strategies to explore whether these two events might be linked. 5-bromouridine 5'-triphosphate (BrUTP) assay to detect incorporation into newly synthesized transcripts (Aoki et al., 1997) revealed that, compared with embryos grown in +P medium, those cultured in -P fail to show any detectable BrUTP staining (Figures 2A–2C). The phosphorylation status of Ser5 or Ser2 on the C-terminal domain of RNA Polymerase II is also an excellent measure of transcription-initiation as RNA Pol II requires these serine phosphorylation events in order to be part of the initiation and the elongation complex, respectively (Egloff and Murphy, 2008). A significant reduction of Pol II Ser-5P and Pol II Ser-2P in -P embryos demonstrates that RNA Pol II is not engaged in transcription at the time of ZGA in +P embryos (Figures 2D–2I). Importantly, total RNA Pol II protein abundance is not affected by pyruvate deprivation (Figures S2A–S2D). Finally, we compared the protein expression of SIRT1, the product of an early zygotic transcript, in +P and -P media. SIRT1 is robustly detected at the 2-cell stage when pyruvate is included in the medium but is eliminated when grown in the absence of pyruvate (Figures 2J–2L). Taken together, we conclude that exogenously supplied pyruvate is essential for activation of the zygotic genome. Lack of ZGA, in turn, is the likely cause of the cell-cycle block since artificially inhibiting DNA replication or cytokinesis does not eliminate ZGA, whereas preventing ZGA will stop the cell from developing beyond the 2-cell state (Schultz, 1993).

Subcellular Localization of Enzymes Involved in Pyruvate Metabolism

Diverse functional assays of oxygen consumption, ATP generation, mitochondrial morphology, and measurement of membrane potential (Acton et al., 2004; Houghton et al., 1996; Trimarchi et al., 2000) have concurred that early stage mitochondria show low energetic activity compared to those in the blastocyst. Also, two distinct classes of early stage mitochondria are identified based on their membrane potential (Acton et al., 2004). As

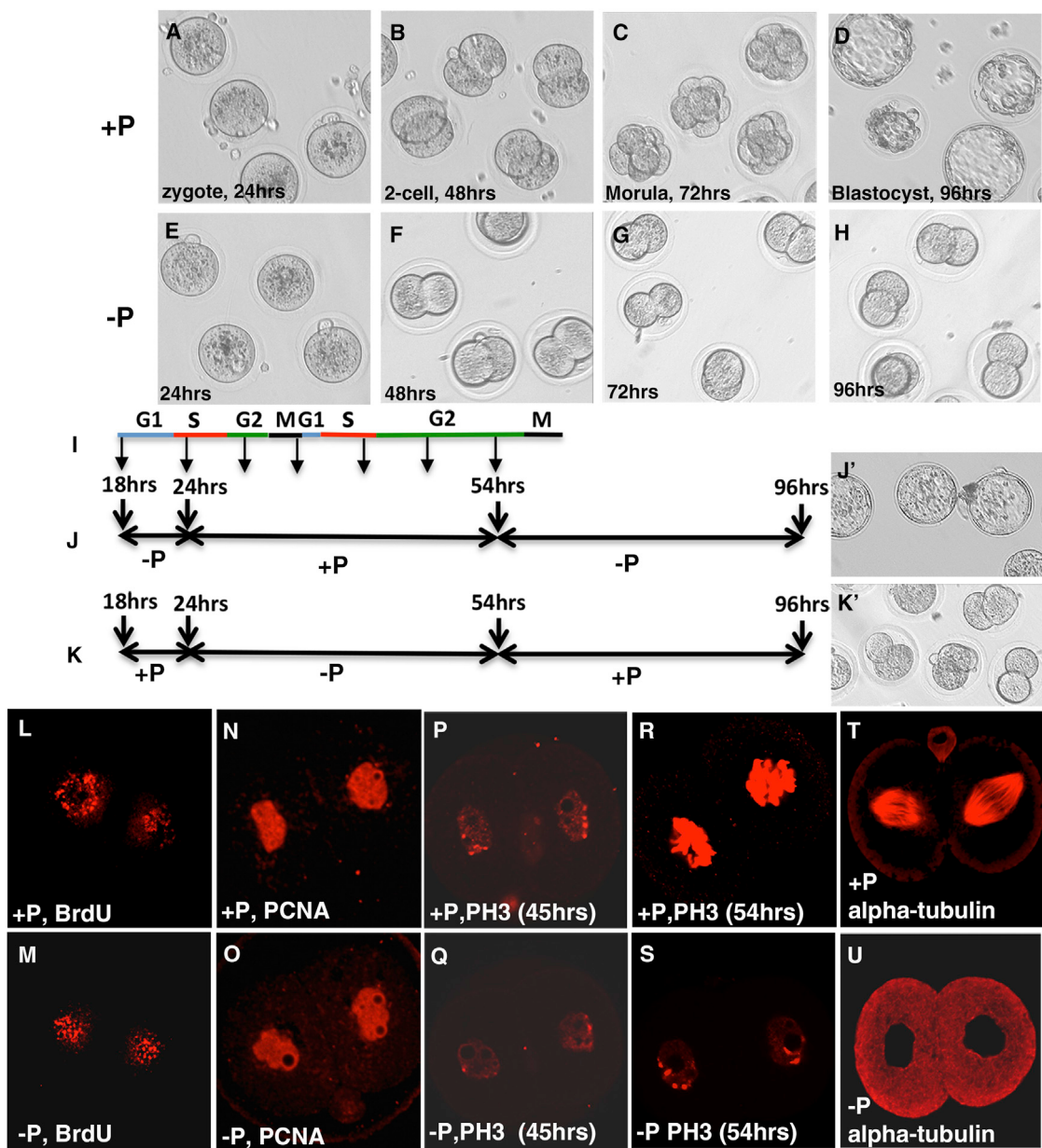


Figure 1. Role of Pyruvate in Early Development

All timings are in hours elapsed following hCG injection. Zygotes are isolated at 18 hr post-hCG and cultured until the specified time post-hCG.

(A–D) Embryos cultured in +P medium as controls at (A) 24-, (B) 48-, and (C) 72-hr morula and (D) 96-hr blastocyst.

(E–H) Embryos cultured in -P medium at (E) 24-hr zygote; (F) 48-hr 2-cell embryo; (G) 72-hr 2-cell arrested, and (H) 96-hr 2-cell arrested.

(I) Cell-cycle phases in 1- and 2-cell embryos (adapted from [Aoki et al., 1997](#)).

(J and J') Zygotes cultured in -P (until 24 hr) and then shifted to +P (from 24 to 54 hr) and then shifted back to -P (54-hr blastocyst); these embryos develop normally and form blastocysts.

(K and K') In the converse experiment, zygotes cultured in -P medium (24–54 hr) and in +P (before 24 hr and after 54 hr) are arrested at the 2-cell stage.

(J–K') 30-hr window (24–54 hr) as necessary and sufficient for pyruvate dependence.

(L–O) Embryos at 38 hr cultured in +P (L) or -P (M) show identical 2-hr BrdU incorporation marking S phase. Similarly, PCNA staining, also marking S phase, is unchanged in +P (N) and -P (O) cultured embryos.

(P–S) G2 phase monitored by PH3 staining shows entry into this phase (at 45 hr) with very faint PH3 staining in both +P (P) and -P (Q) embryos. However at 54 hr, progression through G2 in +P (R) is marked by high PH3 staining, not seen in -P (Q).

(T–U) At 60 hr, tubulin expression highlights spindle assembly in +P (T) and the lack of it in -P (U).

See also [Figure S1](#).

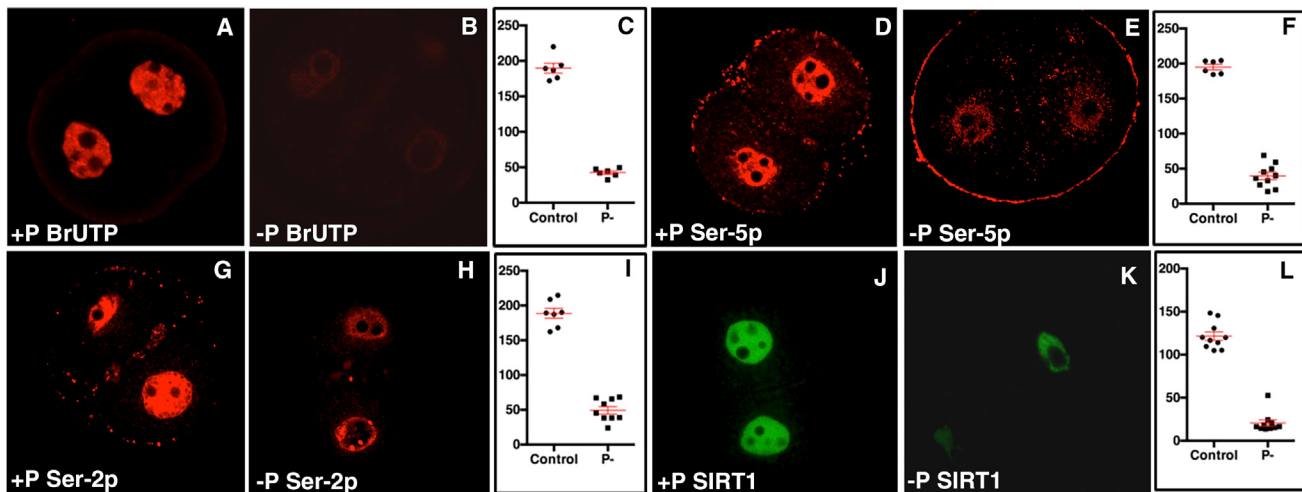


Figure 2. Pyruvate Dependence of Zygotic Genome Activation

All times are in hours post-hCG injection; embryos are isolated at 18 hr and cultured in either +P or -P media until 54 hr post-hCG.

(A–C) +P (A) but not -P (B) grown embryos incorporate BrUTP that marks synthesis of nascent transcripts. (C) $p < 0.0001$ (nuclei n = 6).

(D–I) Phosphorylation of serine moieties at positions 5 and 2 of Pol II is essential for transcription. Both sites are phosphorylated in +P embryos (D and G) but not in -P medium (E and H). $p < 0.0001$ (nuclei n = 10 for 5P and n = 9 for 2P) (F and I).

(J–L) SIRT1 is an early zygotic gene expressed in +P (J) but not in embryos cultured in -P medium (K). $p < 0.0001$ (nuclei n = 10) (L).

Data are presented as the means \pm SEM. See also Figure S2.

culture conditions and genetic backgrounds can affect mitochondrial function (Williams et al., 2016), it was important for us to make sure that these previously well-established conclusions are also seen under our culture conditions. Indeed, we confirmed that when stained with JC1 dye, a small subset of mitochondria along the edge stain red (indicating high membrane potential), while the vast majority stain green (suggesting low membrane potential) (Figures 3A and 3B). Similar results were obtained upon staining with the Ca^{2+} concentration-sensitive dye Rhodamine 2AM, an independent marker of mitochondrial membrane potential (Figure 3D). JC1 and Rhodamine-2AM can penetrate the tissue since extensive mitochondrial staining is readily detected throughout the depth of the embryo at many developmental stages (e.g., Figures S3B and S3C). As further controls, we verified that addition of carbonyl cyanide *p*-trifluoromethoxyphenylhydrazone (FCCP), a mitochondrial membrane un-coupler, causes loss of Rhodamine 2AM staining and conversion of all mitochondrial JC1 staining to green, indicating loss of membrane potential (Figures 3C and 3E).

The absolute requirement of pyruvate for development seems to be at odds with the low bioenergetic activity of the early embryo. We therefore examined the activation status of the mitochondrial enzyme PDH that enables conversion of pyruvate to acetyl-CoA. PDH-kinase (PDK) phosphorylates the PDH-E1 α subunit and renders the PDH enzyme complex inactive (Holness and Sugden, 2003). A corresponding phosphatase, called PDH-phosphatase (PDP), reverts PDH to its active, non-phosphorylated form (Holness and Sugden, 2003). The expression patterns of PDK and PDP can provide valuable information about the activation status of PDH.

In the oocyte, PDK protein is at marginally detectable levels (Figure S3D), increasing somewhat at pronuclear stages PN2–3

and PN4–5 (Figure S3E). Truly robust expression of PDK is evident in the mitochondria of 2-cell embryos (Figures 3F and S3F). It is unusual to see such high PDK levels in non-glycolytic cells, and the resulting attenuation of PDH activity will decrease TCA cycle flux. This is consistent with low bioenergetic activity of the 2-cell embryos.

The activity pattern of PDH can also be directly judged by staining with a series of antibodies. The first, generated against the phosphorylated epitope of PDH-E1 α , specifically recognizes the inactivating phosphorylation site (called α -PDH^{inactive} here). This antibody has been extensively used to detect inactive PDH in both *in vivo* and *in vitro* assays (Donohoe and Bultman, 2012). Staining with α -PDH^{inactive} decorates a majority of the mitochondria in the 2-cell embryo (Figures 3G and S3G–S3I), indicating that mitochondrial PDH is largely inactive. As controls, the PDK blocker dichloroacetate (DCA) suppresses α -PDH^{inactive} staining and raises the mitochondrial Ca^{2+} level (Figures S3I–S3K).

A second antibody, generated against the N-terminal 131 amino acids (31–161) of PDH E1 α protein, recognizes both the active and the inactive forms of the protein (called α -PDH^{total} here; Sutendra et al., 2014). Immuno-staining with α -PDH^{total} reveals that total PDH is localized not only to the mitochondrion, but also prominently in the nuclear compartment (Figures 3H and 3I). Nuclear PDH is not recognized by α -PDH^{inactive} and is therefore un-phosphorylated and likely active. Screening among the large collection of commercially available PDH antibodies, we found one (Tomilov et al., 2014) that specifically recognizes this nuclear component (Figures 3J–3L). We refer to this antibody as α -PDH^{nuc}. This same antibody exclusively stains mitochondria at the blastocyst stage (Figure S3L) as is also true of the α -PDH^{total} staining (Figure 3M) suggesting that α -PDH^{nuc} likely

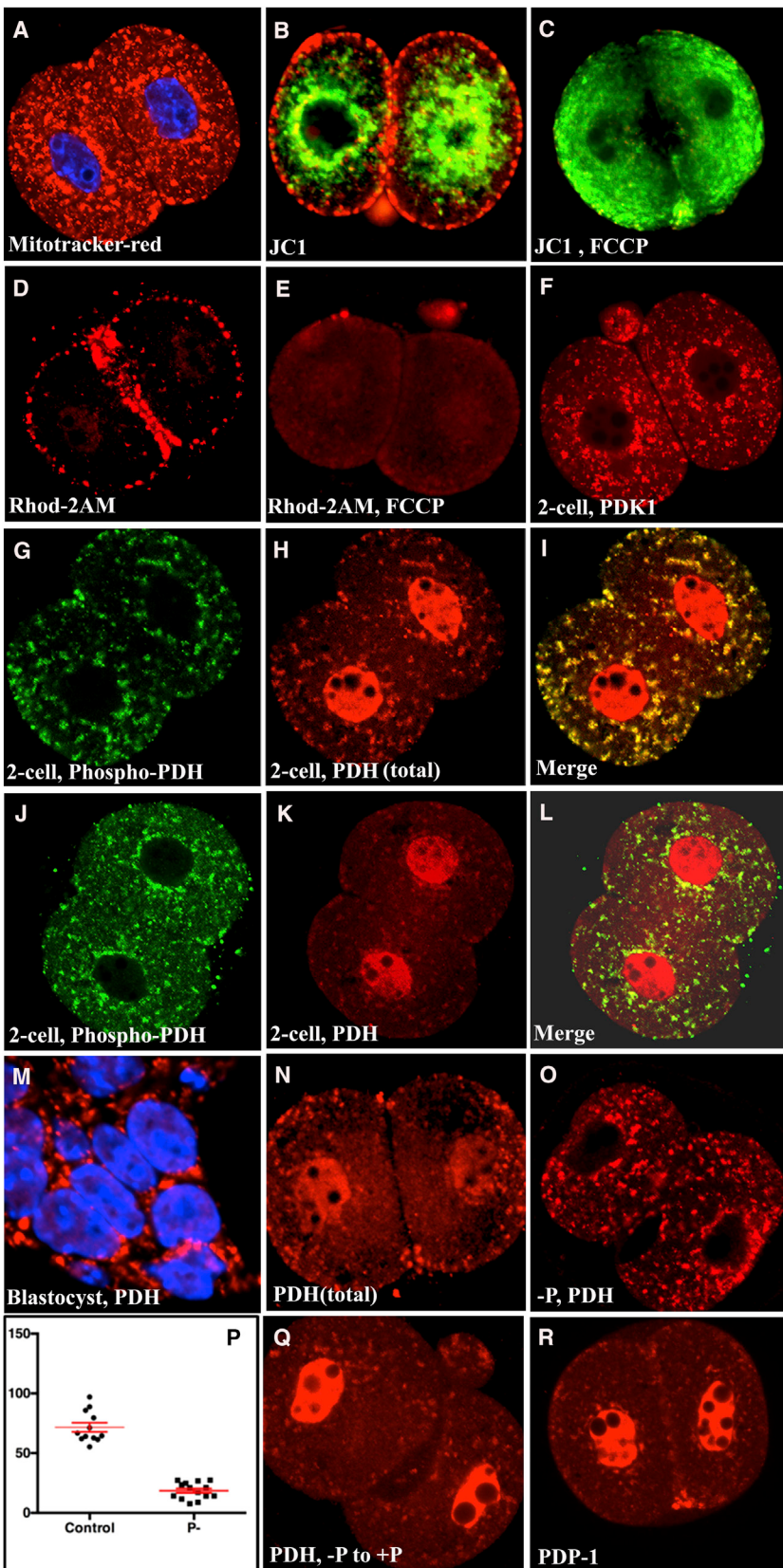


Figure 3. Sub-cellular Distribution of Pyruvate Dehydrogenase Complex

All embryos are at 54 hr post-hCG except where noted.

(A) Mitochondria identified by Mitotracker staining (red).

(B) JC1 dye identifies mitochondria with high (red) and low (green) membrane potential. Low activity and membrane potential for the majority of mitochondria is also revealed by calcium sensing dye (Figure S3A) staining.

(C-E) A 30-min FCCP treatment causes loss of active (red) JC1 staining (C) and a corresponding increase in inactive (green) mitochondria. Similarly, FCCP significantly reduces uptake of the calcium-sensitive mitochondrial dye, Rhod-2AM (compare (D) and (E)). (F) PDK1 (inhibitor of PDH) is first detected in single cell embryos (also, Figures S3D and S3E), rising to high levels at 54 hr.

(G) α -phospho-PDH antibody staining shows that PDH^{inactive} is exclusively mitochondrial.

(H) α -PDH^{total} shows staining in the mitochondrion and the nucleus.

(I) A merge of the images in (H) and (I) establishes that the nuclear component is PDH^{active} (red not green) and the mitochondrial component is PDH^{inactive} (red and green).

(J) Mitochondrial localization of PDH^{inactive}.

(K) The PDH antibody Ab110334 exclusively recognizes the nuclear component.

(L) Merge of images in (J) and (K) indicates that Ab110334 specifically recognizes PDH^{active}.

(M) 96-hr blastocyst, no PDH is detected in the nucleus, and α -PDH^{total} specifically marks mitochondria. This is also true for somatic cell lines (Figure S4A). To-Pro (blue) marks the nucleus.

(N) α -PDH^{total} (Control +P medium) shows dual nuclear and mitochondrial staining.

(O) Nuclear localization is lost in -P medium.

(P) $p < 0.0001$ (nuclei $n = 14$) comparing nuclear signal intensity.

(Q) 66 hr (until 54 hr in -P, then shifted to +P for 12 hr) rescues nuclear localization.

(R) PDP-1 is nuclear and presumably activates PDH. Data are presented as the means \pm SEM. See also Figure S3.

recognizes the active PDH enzyme that is nuclear at the 2-cell and mitochondrial at the blastocyst stage. The E2 and E3 sub-units of PDH also show dual localization to the mitochondrion and the nucleus (Figures S3M and S3N). The nuclear localization of PDH initiates during the S phase of the mitotic cycle based on timing as well as co-localization with PCNA (Figures S3O–S3V). PDH is first detected at PN3 and PN4 stages of the 1-cell embryo. Following mitosis, nuclear PDH is extremely low during the short G1 phase of the 2-cell embryo but is robustly nuclear during the S phase (marked by PCNA staining, Figures S3R–S3V) and in the prolonged G2 phase that follows (Figure S3T). Strikingly, in-vivo-isolated 4-cell embryos occasionally show two of the cells with mitochondrial localization and the other two with largely a nuclear pattern, while other embryos from the same collection show identical, nuclear localization pattern in all four cells (Figures S3W and S3X). As each pair of cells of a 4-cell embryo can be slightly asynchronous in their cell cycle with the other, these results suggest that nuclear localization follows the final cyclic pattern at the 4-cell stage. Also, these images indicate an exchange of the enzyme between the mitochondrial and nuclear compartments.

Pyruvate has multiple roles within the cell. One unexpected role, relevant to the current context, is revealed upon staining with PDH antibodies in a pyruvate-deprived embryo. In contrast to embryos grown in the normal +P medium, those that are grown without pyruvate (−P medium) show a complete lack of nuclear PDH (Figures 3N–3P). Further support for the involvement of pyruvate in nuclear localization is suggested by rescue experiments. Embryos cultured until the late 2-cell stage without pyruvate, when returned to a +P medium, and cultured for an additional 12 hr, show partial rescue of nuclear PDH (Figure 3Q). However, the 2-cell mitotic block is not rescued by this delayed pyruvate addition (data not shown).

Conversion of phosphorylated PDH-E1 α to an active un-phosphorylated form requires pyruvate dehydrogenase phosphatase (PDP). Antibody staining reveals that PDP is localized to the nucleus at the 2-cell stage (Figure 3R). The exclusive localization of PDK to the mitochondrion (Figure 3F) and PDP to the nucleus (Figure 3R) indicates a concerted regulatory mechanism that keeps the mitochondrial PDH relatively inactive and the nuclear PDH complex active at this specific stage of development. Later in the paper, we describe a functional assay directly demonstrating that the nuclear component of PDH is indeed enzymatically active.

Localization of Pyruvate Carboxylase and Enzymes of the TCA Cycle

The metabolite citrate is very abundant in the early mouse pre-implantation embryo compared to that usually seen in somatic cells (Barbehenn et al., 1978). Citrate is generated by the condensation of the metabolites acetyl-CoA and oxaloacetate (OAA). In principle, pyruvate can be converted to acetyl-CoA by PDH; additionally, pyruvate can be directly converted to OAA in the presence of pyruvate carboxylase (PCB) (reviewed in Holness and Sugden, 2003). Indeed, early embryonic PCB activity has been reported in the literature (Quinn and Wales, 1974).

Upon immuno-staining for PCB, we found a fraction of it to be present in the nucleus (Figure 4C). Unlike for PDH, antibodies

that discriminate between active and inactive versions of PCB, or the other enzymes described in this section, are not available. Although the nuclear staining is clearly discernable, the stronger mitochondrial component makes it harder to tell apart from that in the nucleus. We followed four steps to establish nuclear localization. First, we isolated and immediately fixed single nuclei from the embryos (see STAR Methods), stained them with the antibody and with DAPI, and imaged them directly. This would prevent any artifacts due to spillover staining or saturation issues with microscopy due to the dominant mitochondrial staining. Second, to ensure that the nuclear staining is not an artifact of the ex vivo culture system, we isolated older, 2-cell embryos instead of zygotes, directly from the mother by adjusting the collection time, and fixed and stained them with no time spent in culture. Third, we cultured embryos in +P and −P media followed by immunohistochemistry to determine whether the enzyme, as for PDH, requires pyruvate for nuclear localization. Finally, we repeated our staining protocol on multiple embryos to quantitate the strength of staining with and without the presence of pyruvate.

Following this protocol, we determined that isolated nuclei show the presence of PCB (Figures 4A and 4A'), 2-cell embryos from in vivo collection show nuclear localization (Figure 4B) similar to that seen following culture in +P medium (Figure 4C), and that the nuclear localization of PCB is entirely pyruvate dependent (Figure 4C'). Quantitation of multiple isolates clearly established that the pyruvate dependence is statistically significant (Figure 4C'). In principle, nuclear PCB and PDH could metabolize pyruvate to generate OAA and acetyl-CoA, respectively, in the nucleus. To make citrate, however, involves the enzyme citrate synthase (CS) that is a component of the TCA-cycle not known to have any extra-mitochondrial function. Nevertheless, following the four steps elaborated above for PCB, we found that a fraction of the CS enzyme also localizes to the nucleus (Figures 4D–4F) in a pyruvate-dependent manner (Figures 4F–4F'). While nuclear localization of PDH has been reported in other systems (Chueh et al., 2011; Sutendra et al., 2014), nuclear localization of a TCA cycle enzyme such as citrate synthase is an unexpected finding and led us to investigate the 2-cell embryo localization status of all TCA cycle enzyme isoforms that normally function in the mitochondrion. Beyond CS, the next TCA cycle step uses the mitochondrial enzyme aconitase 2 (ACO2) to metabolize citrate to iso-citrate. ACO2 expression is distinctly nuclear in a pyruvate-dependent fashion at the 2-cell stage (Figures 4G–4I'). Next is the enzyme mitochondrial isocitrate dehydrogenase (IDH3), which uses isocitrate as a substrate to generate α -ketoglutarate (α -KG), an important metabolite required for DNA and histone demethylation enzyme function (Xiao et al., 2012). IDH3 is also nuclear at this stage of development only in the presence of pyruvate (Figures 4J–4L'). None of the above enzymes is nuclear at later stages such as in the blastocyst where the same antibodies detect them exclusively in the mitochondrion (Figures 4M–4P). The next set of TCA cycle enzymes is either detected at very low levels in the nucleus (KGDH, Figures 4Q and 4Q') or not detected (succinyl Co-A synthetase [SCS], succinate dehydrogenase A [SDHA], malate dehydrogenase 2 [MDH2]) in the nucleus at all (Figures 4R–4T') even in the presence of pyruvate. Finally, embryos isolated after

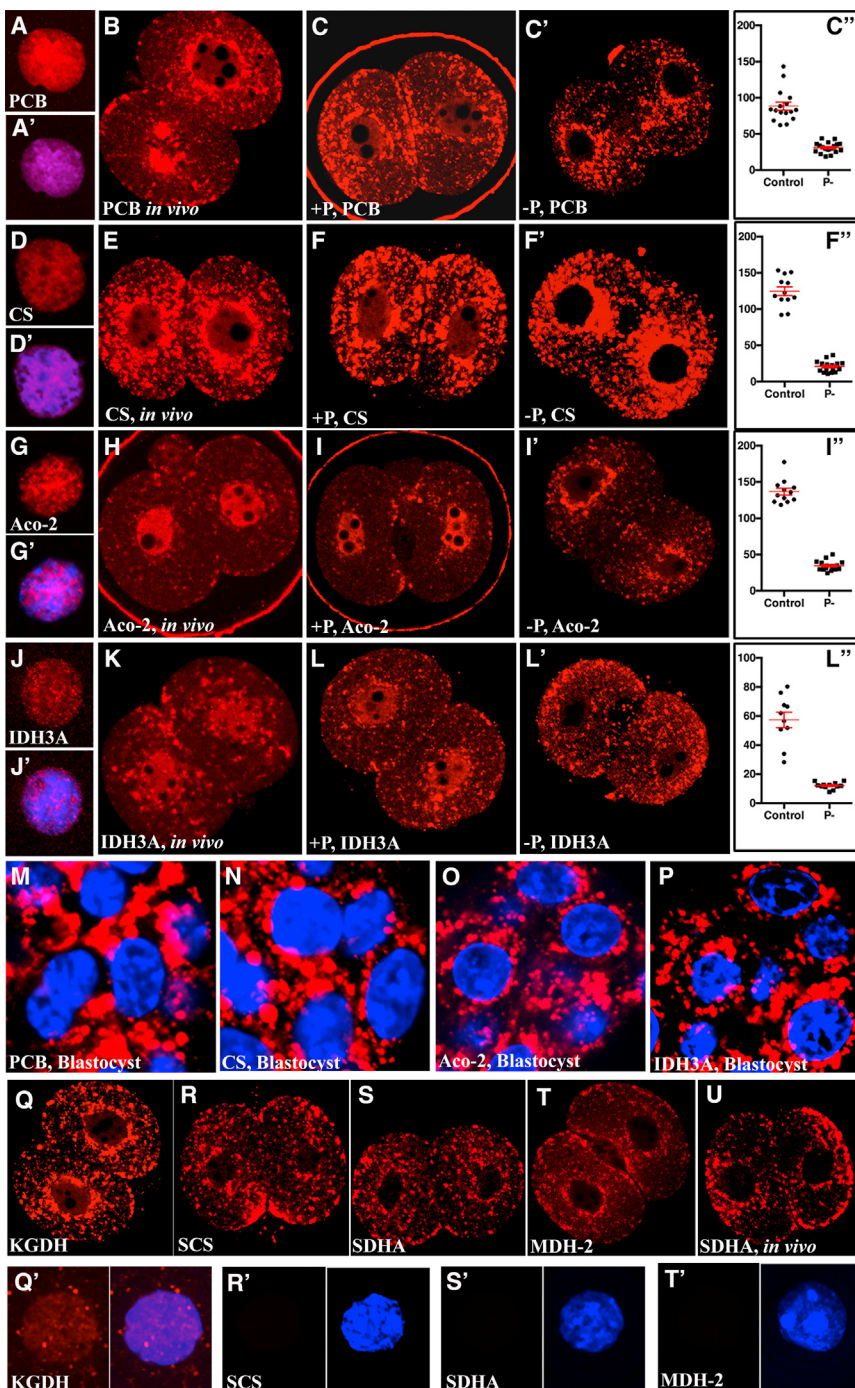


Figure 4. Sub-cellular Localization of TCA Cycle Proteins

(A–L'') Nuclear localization of a subset of TCA-cycle-related (class 1) enzymes. (A, D, G, and J) Nuclei isolated from 54-hr +P embryos, fixed, and then stained with indicated antibodies. (A', D', G', and J') The same nuclei are shown, including the To-pro channel (blue). (B, E, H, and K) Embryos allowed to develop *in vivo* during the pre-implantation phase until late 2-cell stage and stained with the indicated antibodies without any in vitro culture. (C, F, I, and L) Embryos cultured in medium containing pyruvate (+P). (C', F', I', and L') Embryos cultured in medium lacking pyruvate (-P). (C'', F'', I'', and L'') Quantitation of data comparing intensity of nuclear staining in (+P) and (-P) grown embryos. In all four instances, p value is <0.0001(nuclei n = 18 PCB, n = 16 for CS, n = 16 for Aco-2, and n = 12 for IDH3A). Clear evidence for pyruvate-dependent nuclear localization is evident for the enzymes pyruvate carboxylase (PCB) (A–C''), citrate synthase (CS) (D–F''), mitochondrial aconitase-2 (Aco-2) (G–I''), and mitochondrial isocitrate dehydrogenase 3A (IDH3A) (J–L'').

(M–P) Embryos cultured to the blastocyst stage in +P medium and stained with antibodies against, PCB (M), CS (N), Aco-2 (O), and IDH3A (P). In each case, the respective TCA-cycle-related, class I enzyme is exclusively mitochondrial with no nuclear component detected at this late developmental stage. Nuclei (blue) are marked with To-Pro. (Q–T') Sub-cellular and nuclear localization of the next series of TCA enzymes in +P cultured embryos. None of these enzymes is seen in the nucleus: α -ketoglutarate-dehydrogenase (KGDH) (Q and Q'), succinyl Co-A synthetase (SCS) (R and R'), succinate dehydrogenase A (SDHA) (S and S'), and mitochondrial malate dehydrogenase-2 (MDH-2) (T and T') are exclusively localized to the mitochondria with no detectable staining seen in the nucleus.

(U) SDHA expression is specifically mitochondrial in late 2-cell stage allowed to develop *in vivo* until this later time and stained with no ex vivo culture of the embryos.

Data are presented as the means \pm SEM. See also Figure S4.

tional protein translation machinery is equally essential for maintaining the mitochondrial and the nuclear levels of PDH (Figures S4O and S4P). We propose that, in addition to its role in maintaining energy homeostasis, mitochondrial pyru-

vate plays an independent role in facilitating the enzyme complex transport process. This model is supported by additional experiments, discussed later in the paper.

In summary, in the 1- to 2-cell stages of mouse pre-implantation embryo, half of the TCA cycle proteins, CS, ACO2, IDH3, and also PDH, PCB are readily detected in the nucleus (in addition to the mitochondria). Collectively, we designate these as class I (TCA cycle related) enzymes, whereas the enzymes that function

in vivo development to the 2-cell stage and then immediately fixed and stained with SDHA antibody gave no detectable signal in the nucleus, as was seen for the cultured embryos (Figure 4U). Important positive and negative specificity controls are described in Figure S4.

Nuclear transport of the TCA-cycle-related enzymes not only requires the presence of pyruvate, but requires mitochondrial entry of the supplied pyruvate (Figures S4M and S4N). A func-

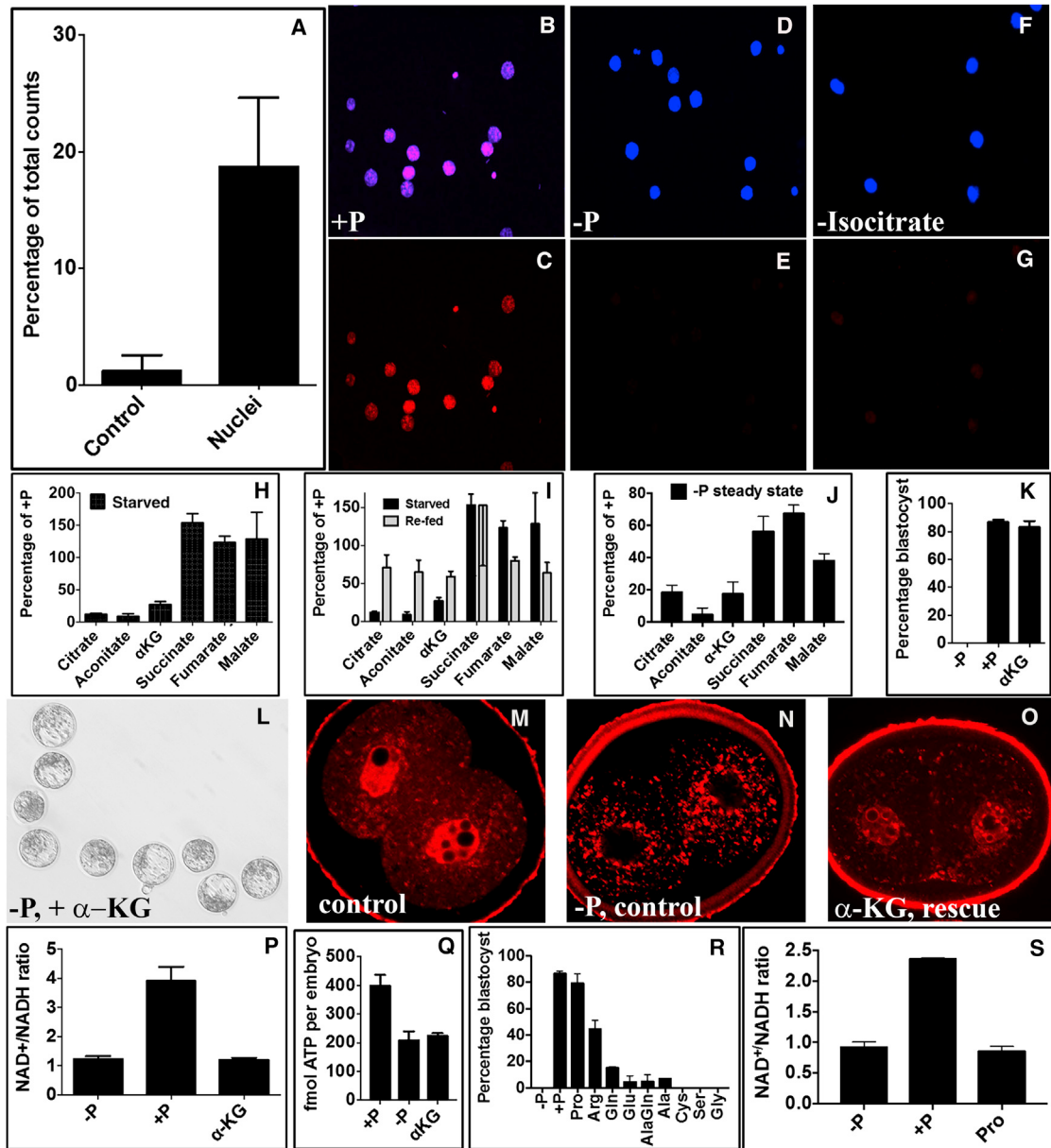


Figure 5. Functional Characterization of Pyruvate Metabolism in Early Embryos

(A) Generation of $^{14}\text{CO}_2$ from $1\text{-}^{14}\text{C}$ -pyruvate by nuclei isolated from two-cell embryos ($p = 0.04$, $n = 3$, each biological replicate comprises 200 nuclei).

(B–G) Isocitrate dehydrogenase activity in nuclei isolated from 2-cell embryos. DAPI (blue) identifies individual nuclei, fluorescence generated by reduction of cyano-tetrazolium dye is indicative of IDH activity and is shown in red. (B and C) Nuclei ($n = 76$) from +P embryos assayed in complete assay solution are positive for IDH activity (red). (D and E) Nuclei ($n = 86$) from -P embryos assayed in complete assay solution; absence of signal in (E) confirms pyruvate dependence. (F and G) Nuclei ($n = 72$) from +P embryos evaluated in assay solution without isocitrate; absence of signal in (F) shows specificity of the assay for IDH that converts isocitrate to α -KG.

(H) 2-cell embryos are starved for 30 min in medium lacking pyruvate, lactate, and glucose. Metabolite levels are compared to control embryos moved for 30 min to a fresh medium including pyruvate but lacking glucose and lactate. Citrate ($p = 0.021$), aconitate ($p = 0.0056$), and alpha-ketoglutarate ($p = 0.0098$) levels in starved samples are significantly lower than in control. In contrast, succinate levels increase ($p = 0.0087$) and malate ($p = 0.35$) and fumarate levels do not change ($p = 0.25$). Data are presented as the means \pm SD; $n = 3$; each biological replicate contains more than 200 embryos.

(I) Starved embryos are re-fed with pyruvate for 20 min. Citrate ($p = 0.0039$), aconitate ($p = 0.0038$), and alpha-ketoglutarate ($p = 0.0026$) levels recover (increase) significantly following re-feeding. In contrast, re-feeding has little effect on succinate ($p = 0.99$) and malate ($p = 0.061$) and even caused a significant drop for fumarate ($p = 0.002$). Data are presented as the means \pm SD; $n = 3$; each biological replicate contains more than 200 embryos.

(J) Pyruvate dependence of TCA cycle metabolite levels at 48 hr. The steady-state levels of all metabolites are lower in -P compared with +P control. However, the drop in citrate, aconitate, and α -KG levels is more substantial than that seen for succinate, fumarate, and malate. Data are presented as the means \pm SD, $n = 3$, with each replicate containing at least 100 embryos.

(legend continued on next page)

later in the TCA cycle that we call class II enzymes remain strictly mitochondrial. Given the low activity of the TCA cycle, in the mitochondrion, in principle, nuclear localization of class I enzymes affords the ability to generate metabolites: acetyl-CoA, citrate, isocitrate, and α -KG that are important for ZGA directly within the nucleus. Collectively, we call them class I metabolites. The products of the class II enzymes (class II metabolites) should present a very different profile in the context of 2-cell development. This was next tested by multiple assays for enzyme function and metabolite levels.

Activity Assays in Isolated Nuclei for Key Mitochondrial Enzymes

We have shown that nuclear PDH complexes are largely unphosphorylated and therefore predicted to be catalytically active. The first step in this enzymatic activity involves the decarboxylation of pyruvate and generates CO_2 derived from the carbon at position 1 of pyruvate. To directly assay this activity, we adapted a technique previously described for larger sample sizes (STAR Methods; Sies et al., 1983; Williamson et al., 1979) to work with isolated nuclei from 2-cell embryos (Figure 5A). This direct enzymatic assay demonstrates active decarboxylation of pyruvate within the nuclei. Combined with the observation that nuclear PDH remains un-phosphorylated, the labeling assay allows us to conclude that PDH detected in the nucleus is catalytically active. Consistent with these results, lipoic acid modification, essential for PDH complex function, is detected in the nucleus in the presence of pyruvate (Figures S5A and S5B).

IDH3 is the last of the class I enzymes, and it converts isocitrate to α -KG, in the process generating NADH from NAD^+ . The production of NADH was monitored using a nitro-tetrazolium dye (cyano-tetrazolium), which fluoresces red and precipitates upon reduction (Dikov et al., 2004). Embryos cultured in the +P but not -P medium have active IDH3 in their nuclei (Figures 5B–5E). Importantly, the IDH3 signal requires the presence of isocitrate and NAD^+ (Figures 5F and 5G) (but not NADP^+ ; see STAR Methods) in the assay solution reaction. Thus, key class I mitochondrial enzymes are catalytically active within the nuclei of 2-cell embryos.

Metabolite Measurements

Classic cycling assays (Barbehenn et al., 1978) have suggested that metabolite dynamics in glycolysis can be efficiently analyzed by starving cells for a short period of time to measure changes and then re-feeding them to estimate metabolite recovery. Adapting this assay for measuring TCA cycle metabolites

using a highly sensitive capillary ion chromatography method for separation, followed by high-resolution mass spectrometry (see STAR Methods), we were successful in measuring small quantities of most TCA cycle metabolites in approximately 300 embryos. Metabolite levels were measured (1) following incubation in +P medium with no starvation, (2) after a brief 30-min starvation in medium lacking glucose, pyruvate, and lactate, and (3) following 20-min recovery in medium containing pyruvate (but not lactate and glucose). Of the TCA cycle metabolites, citrate, aconitate, and α -KG levels are significantly reduced upon starvation and significantly restored during the short, 20-min, re-feeding session (Figures 5H and 5I). Remarkably, succinate, fumarate, and malate, which are generated by enzymes that are not localized to the nucleus, are not diminished following starvation nor do their levels rise following re-feeding with pyruvate (Figures 5H and 5I). The observation that malate levels, in fact, fall upon re-feeding is in agreement with earlier observations (Barbehenn et al., 1978).

In a second analysis, we isolated zygotes, cultured them until the 2-cell stage under +P and -P conditions and then directly measured TCA cycle metabolites. Figure 5J shows that metabolites formed by enzymes present in the nucleus decrease significantly more in -P medium than metabolites formed by enzymes that are exclusively mitochondrial. Collectively, these data demonstrate that the TCA metabolites have different dynamic properties. Those generated by enzymes with a nuclear component are more dependent on the presence of exogenously provided pyruvate compared with metabolites generated by the later enzymes of the TCA cycle that are not detected in the nucleus.

Rescue Experiments

α -KG is the terminal class I metabolite and in principle capable of producing earlier ones by conversion to citrate. Amazingly, we found that a cell-permeable analog of α -KG added to the -P medium supports development to the blastocyst stage and completely rescues the 2-cell block as well as transport of class I enzymes to the nucleus (Figures 5K–5O).

Metabolite measurements show that the GSH/GSSG ratio, indicative of oxidative stress is unchanged in the absence of pyruvate (Figure S5G). However, the ATP/ADP ratio (Figure S5F), the amount of ATP (Figure 5Q), and the NAD^+/NADH ratio (Figure 5P) are all affected if the growth medium lack pyruvate. Under normal growth conditions, these ratios are critical for embryonic development, and the redox ratio, in particular, is too low in the absence of pyruvate to support progress beyond the 2-cell

(K–O) Percentage of 120-hr embryos forming blastocysts in a -P medium supplemented with a membrane permeable form of 1 mM α -KG. n = independent isolations with each isolation containing least ten embryos. -P n = 10, +P n = 24, α -KG n = 9 (K). Representative examples of α -KG rescued 96-hr blastocysts (L). (M–O) A fraction of PDH is nuclear in +P (M) but not -P (N) cultured embryos. Nuclear localization is restored in -P medium supplemented with α -KG (O). (P and Q) Neither the lowered NAD^+/NADH ratio (n = 5 cycling assays) (P) nor the lowered ATP concentration (Q) in pyruvate-deprived embryos is rescued by α -KG supplementation of -P medium even as developmental and nuclear localization defects (K–O) are completely rescued. p values: +P to -P (p = 0.0199). +P to α -KG (p = 0.0125). -P to α -KG (p = 0.6355). n = 3 independent isolations of embryos.

(R) The percentage of 120-hr embryos forming blastocysts following culture in -P medium supplemented with each indicated amino acid (1 mM). Proline fully and arginine partially rescue the pyruvate defect. n = independent isolations, with each isolation containing least ten embryos. -P n = 10, +P n = 24, proline n = 8, arginine n = 6.

(S) The lowered NAD^+/NADH ratio upon pyruvate deprivation is not rescued by proline supplementation (n = 4 cycling assays). Thus, pyruvate-deprived embryos continue to be under energetic and redox stress with supplemented α -KG, even as the 2-cell block and ZGA are rescued.

Data are presented as the means \pm SEM, unless otherwise stated. See also Figure S5.

stage. Interestingly, and somewhat unexpectedly, we found that the embryos rescued with α -KG-supplemented -P medium continue to exhibit reduced NAD⁺/NADH ratio (Figure 5P) and reduced ATP levels (Figure 5Q) similar to embryos cultured in -P media rather than those grown in +P. Thus, α -KG does not rescue the developmental phenotype by lessening the changes in energetic or redox balance due to the absence of pyruvate. It is doing so by providing the essential carbon, normally provided by pyruvate, required for downstream anabolic processes.

Within the cell, catabolism of amino acids can generate α -KG. We therefore asked whether non-essential amino acids rescue -P embryo phenotypes. Interestingly, the only two that are capable of such a rescue are proline and arginine, both known to generate α -KG (Figures 5R, S5C, and S5D). None of the other non-essential amino acids substantially rescues the phenotype, including alanine and serine that can generate pyruvate (Figure 5R). Similar to α -KG, proline does not rescue the NAD⁺/NADH ratio or ATP levels while rescuing the 2-cell block, once again demonstrating that early embryos can develop into blastocysts even under redox (Figures 5P and 5S) and energetic stress (Figures 5Q and S5C–S5E).

Role of O-linked Glycosylation in Nuclear Localization

Figure 6A summarizes our results thus far that establish that a fraction of class I mitochondrial enzymes are transiently nuclear producing class I metabolites favorable to epigenetic changes that lead to genome activation. Class II enzymes are not similarly dynamic in producing class II metabolites (Figure 6A). The mechanism for moving large enzyme complexes from the mitochondrion to the nucleus is not fully clear (see Discussion), but our data point to an important role for O-linked glycosylation in this process. In +P media, O-glycosylated proteins are located inside the nucleus and on the nuclear membrane (Figure 6B). The localization inside the nucleus is virtually eliminated in -P embryos with the nuclear membrane component relatively unchanged (Figures 6B–6D). Although the majority of nuclear protein import relies on canonical nuclear localization signals (NLSs), other mechanisms exist (Lange et al., 2007). For example, an alternative mechanism involves O-linked glycosylation of the transported protein, followed by binding to a chaperone molecule such as Hsp90 or Hsp70, and the subsequent transport of this complex through the heavily glycosylated pores on the nuclear membrane (Guinez et al., 2005; Duverger et al., 1996). The enzyme necessary for transferring the O-glycosyl moiety derived from UDP-GlcNAc to the target protein is O-linked N-acetylglucosamine transferase (OGT). In +P medium, OGT is seen in the nucleus, as well as in cytoplasmic punctae, but in -P embryos, OGT is no longer nuclear (Figures S6A–S6F). Additionally, the inhibitor STO45849 that specifically blocks OGT function causes loss of PDH nuclear localization (Figures 6E–6G), a reduction in O-glycosylation and a 2-cell block (Figures S6M–S6P). The chaperon proteins HSP70 and HSP90 are prominently expressed at this stage (Figures S6G and S6H), and most strikingly, a specific inhibitor of HSP90, 17-AAG, gives rise to a 2-cell block in development (Figures S6Q–S6T) and prevents nuclear localization of PDH (Figures 6H–6J). Thus, one potential model is that pyruvate-dependent acetylation of glucosamine-6-phosphate is a key step in the formation of O-glycosylated mitochondrial en-

zymes that utilize a chaperone-dependent transport process to locate within the nucleus (see Discussion for alternatives).

Pyruvate-Dependent Histone Modifications

A number of epigenetic changes linked to genome activation will require appropriate metabolites that help add or delete acetyl or methyl groups to histones (Martinez-Pastor et al., 2013). We find that pyruvate-deprived embryos show a virtual elimination of H3K4 acetylation (Figures 6K–6M), a reduction in H3K27 acetylation (Figures 6N–6P), and an almost complete elimination of H3K27 trimethylation (Figures 6Q–6S). Global acetylation of other sites such as H3K9, H3K14, or H4K5 or trimethylation of H3K4 and H3K9 remains unchanged (Figures S6U–S6X').

PDH Localization in Human Embryos

The surprising finding that the first half of the mouse TCA cycle enzymes are detected in the nucleus at the 2-cell stage led us to investigate whether a similar mechanism might operate in human embryos. A conserved mechanism would be relevant to human fertility and in vitro fertilization protocols, and we were therefore granted access to a small number of human embryos from fertilization clinics, through a fully consented and documented process. Due to the very limited tissue availability, we have restricted our study to the localization of PDH to serve as a guide. A mixture of two sets of antibodies, described earlier, was used: α -PDH^{inactive} (recognizes only the inactive phosphorylated version) and α -PDH^{total} (recognizes both active and inactive forms). Unlike in mouse, neither 1-cell pronuclear fusion stage (Figures 7A–7C) nor 2-cell stage (Figures 7D–7F) human embryos show any evidence of nuclear PDH. Similar to that seen in mouse, mitochondrial PDH detected in the human embryo is largely phosphorylated (inactive). At the 4-cell and peaking at the 8-cell stage, a burst of nuclear PDH^{active} becomes readily detectable (Figures 7G–7R), and a single stage later, in the morula, there is no longer a hint of nuclear PDH^{active} in the human embryo (Figures 7S–7U). Thus, in mouse embryos, nuclear PDH initiates at 1-cell, peaks at 2-cell and starts declining beyond the 4-cell stage. In contrast, human embryos initiate nuclear PDH localization at the 4-cell stage, peaking at the 8-cell stage, and is excluded from the nucleus in the morula. Nuclear PDH is never detected in the morula or blastocyst of either mammal. Remarkably, the delayed nuclear entry in the human compared to the mouse embryo corresponds exactly to the natural ZGA timing, which takes place in the mouse, at the late 2-cell stage, and in humans, between the 4-cell and 8-cell stages (Niakan and Eggan, 2013; Xue et al., 2013).

DISCUSSION

This paper investigates the relationship between the metabolic status and developmental progression of mouse pre-implantation embryos. The central finding is that multiple TCA cycle and associated enzymes are temporarily localized to the nucleus, while also maintaining a mitochondrial pool. Functional analysis indicates that such proteins (class I enzymes) are enzymatically active within the nucleus. These enzyme complexes are the ones that belong to the first half-cycle of the TCA cycle, and the data support a model in which they are important

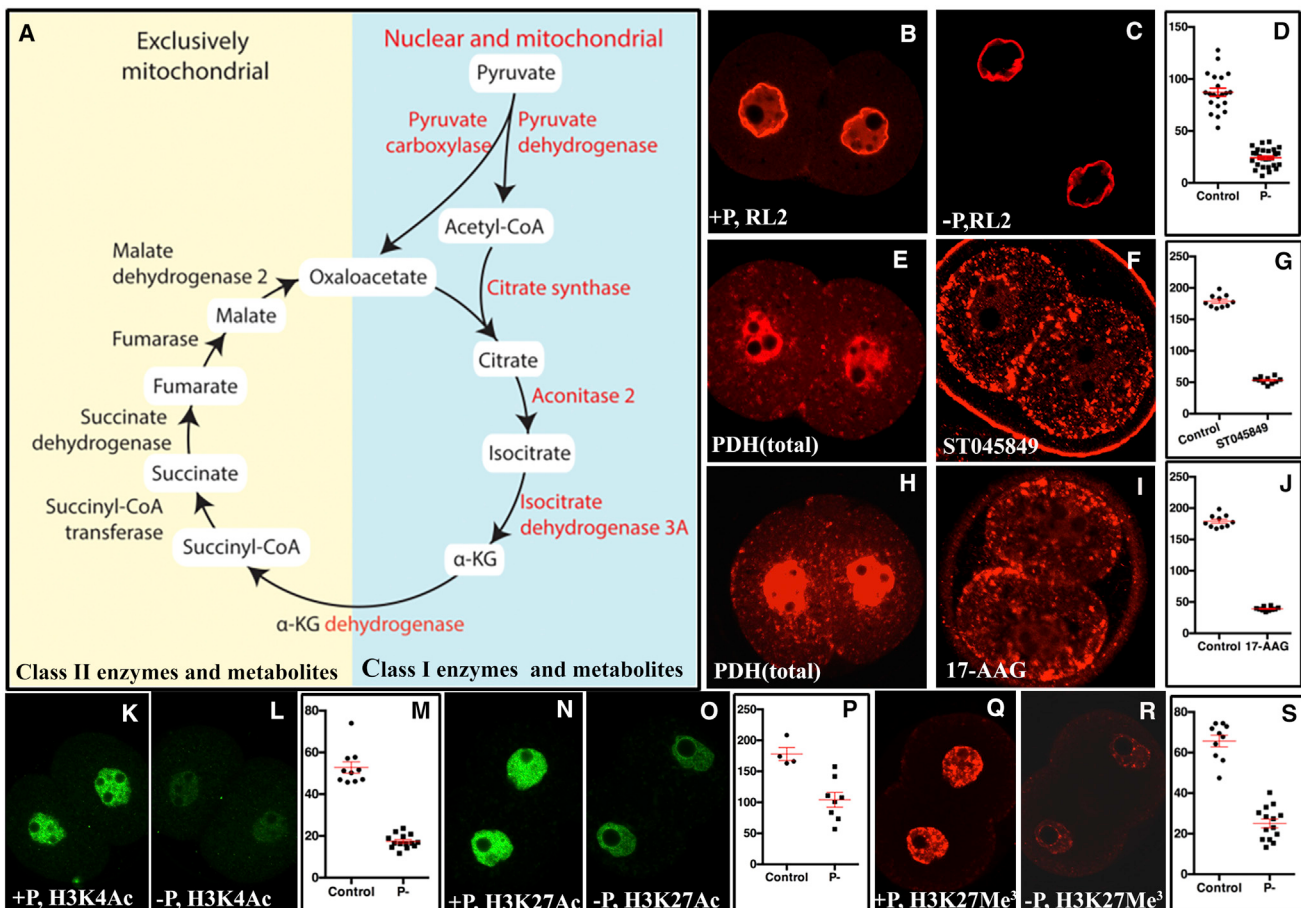


Figure 6. Regulation of Nuclear Import and Its Role in Epigenetic Reprogramming

(A) Schematic representation of the TCA-cycle-related enzymes (blue background) that are detected in the nucleus (class I enzymes), and their corresponding metabolites (class I metabolites) are essential for ZGA and development beyond 2-cell embryo. Contrasted in yellow background are class II enzymes that are never nuclear, and therefore class II metabolites are less dynamic in their response to starvation and low pyruvate.

(B–D) O-linked glycosylation assayed by RL2 antibody in +P shows intra-nuclear and nuclear membrane staining (B). –P embryos (C) show a significant reduction of O-glycosylation in the nucleoplasmic component. $p < 0.0001$ (nuclei $n = 27$) (D).

(E–G) The OGT inhibitor, ST045849, blocks nuclear accumulation of PDH (E and F). $p < 0.0001$ (nuclei $n = 10$) (G).

(H–J) 17-AAG specifically blocks HSP90 function and causes loss of nuclear PDH (H and I). $p < 0.0001$ (nuclei $n = 10$) (J). Consequently, both inhibitors cause a 2-cell block (Figures S5M–S5T).

(K–M) Robust H3K4 acetylation is seen in +P (K) but not in –P (L) embryos. $p < 0.0001$ (nuclei $n = 14$) (M).

(N–P) H3K27 acetylation (N) is partially suppressed in –P medium (O), $p = 0.0027$ (nuclei $n = 8$) (P).

(Q–S) H3K27 trimethylation in embryos cultured in +P (Q) is significantly reduced in –P (R) medium. $p < 0.0001$ (nuclei $n = 14$) (S). All other acetylation and trimethylation marks tested remain unchanged (Figures S6U–S6X).

Data are presented as the means \pm SEM. See also Figure S6.

contributors of metabolites (class I metabolites) such as acetyl-CoA and α -KG essential for epigenetic control and activation of the zygotic genome during the 1- to 2-cell stage of pre-implantation development (Figure 6A). The enzymes in the second half of the TCA cycle (class II enzymes) are not seen in the nucleus and their corresponding class II metabolites such as succinate and fumarate are not favorable for genome activation (Xiao et al., 2012). Strong support for the model is provided by the rescue of the developmental and transport defects due to pyruvate deprivation by exogenously provided α -KG.

Our results show that, at the 1- and 2-cell stages, PDH (that converts pyruvate to acetyl-CoA) is localized both to the mito-

chondrion and the nucleus. The enzyme PDK (that inactivates PDH) is localized to the mitochondrion, while PDP (the activator of PDH) is largely confined to the nucleus. The simplest explanation is that the PDK in the mitochondrion renders PDH less active than at later stages of development, while the PDH that enters the nucleus is activated by PDP. The most significant finding of this paper is that multiple enzymes of the TCA cycle and additional proteins related to entry into the TCA cycle: pyruvate carboxylase, pyruvate dehydrogenase, pyruvate dehydrogenase phosphatase, citrate synthase, aconitase-2, and isocitrate dehydrogenase 3A (class I enzymes) are all transiently seen in the nucleus. The nuclear localization of TCA components is not

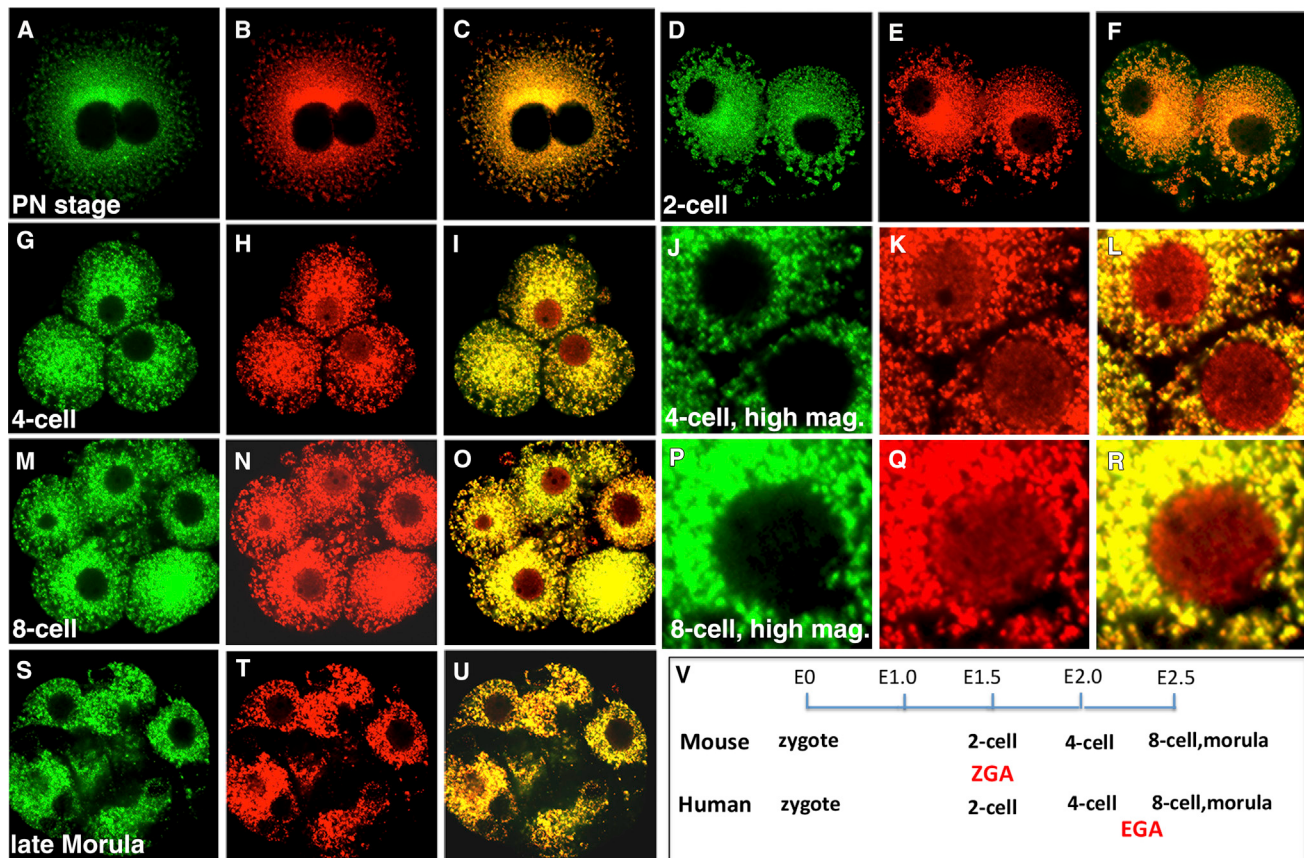


Figure 7. PDH Localization in Pre-implantation Human Embryos

α -PDH^{inactive} staining is shown in green, and α -PDH^{total} staining is in red. In the merged images, overlap (yellow) represents PDH^{inactive} and any non-overlap (red) demarcates PDH^{active}.

(A–F) Unlike in mice (Figure S3Q), no nuclear PDH is detected in the human embryo at either the late 1-cell pro-nuclear fusion stage (A–C) or at the 2-cell stage (D–F). PDH is mitochondrial and largely inactive (yellow).

(G–R) At the 4-cell stage (G–L) and 8-cell stage (M–R), embryos show clear evidence for active PDH in the nucleus (red not green), while PDH^{inactive} (red and green) is restricted to the mitochondrion.

(S–U) A single stage later, in the morula, there is no trace of PDH left in the nucleus.

(V) Nuclear localization of PDH, initiating at the late 1-cell stage in mouse and 4-cell stage in humans, closely correlates with the timing of zygotic/embryonic genome activation: 2-cell stage in mouse, 8-cell stage in humans.

an artifact of the ex vivo culture conditions since identical results are obtained from embryos isolated at different stages of in vivo development and never subject to the ex vivo culture conditions.

Enzyme activity assays adapted for very small number of isolated nuclei established that the enzyme complexes PDH and IDH3, the initiating and terminal class I enzymes are active inside the nucleus. Both dynamic measurements following brief pyruvate starvation and re-feeding as well as steady-state measurements in the presence and absence of pyruvate show a clear distinction in the dynamic property and pyruvate responses of class I and class II metabolites.

Nutrients such as pyruvate are essential for many independent functions within the cell. In this context, the rescue of ZGA and post-2-cell development by α -KG provides a unique perspective. The cells deprived of exogenously provided pyruvate continue to be under redox and energetic stress and yet are able to proceed through ZGA when α -KG is supplied. It is pertinent that the rescue

by α -KG requires the presence of lactate. This observation suggests that lactate can be utilized in the absence of pyruvate, but, due to the low NAD⁺/NADH ratio, the rate of lactate to pyruvate conversion is not sufficiently high to maintain class I metabolite levels. Currently, it is unclear at which point the perturbed NAD⁺/NADH ratio limits lactate utilization. It is likely that the conversion of lactate to pyruvate by LDH is affected, but it is also possible that subsequent steps of the pathway are also limited. The decrease in the levels of class I metabolites will compromise the important biosynthetic and signaling processes that drive developmental progression and are fueled by carbon from lactate and pyruvate. The provision of exogenous α -KG supplies a portion of the carbon requirement of these processes, rendering the redox state less critical, allowing the embryos to progress beyond the 2-cell stage even under energetic or redox stress. It is surprising that proline is able to rescue development, but glutamine is not. Our preliminary (unpublished data) metabolite measurements

suggest that exogenously provided α -KG or proline raises glutamate level in the embryo, but, for reasons still unclear, providing glutamine is much less effective in causing this change.

Most strikingly, we also detect active (unphosphorylated) PDH in the nucleus of human embryos at a stage that is different from that seen in mouse, but one that precisely matches the timing of genome activation in humans. Thus, this entire process linking nuclear localization of TCA enzymes to ZGA seems to be conserved. But this also raises some difficult questions. Our first-level model was that class I enzyme entry into the nucleus aids in ZGA. The human embryo results suggest instead that some other signaling event marking ZGA timing instructs pyruvate-dependent nuclear transport. The simplest model for the trigger would be one that responds to nutrition levels, but this needs to be investigated further.

TCA enzyme complexes are large and require complex folding patterns. Several possible models, to be investigated in the future, can be proposed for the mechanism of their transport to the nucleus. The recently characterized “mitochondrial-derived vesicles” (MDVs) (Sugiura et al., 2014) could play a role in this process. These vesicles facilitate translocation of mitochondrial matrix proteins to several organelles including peroxisomes and lysosomes. While a possible involvement of MDVs in nuclear transport has not been explored, electron microscopy (EM) studies have shown that the early embryo displays a ring of mitochondria closely apposed to the nucleus and displaying a “blebbing” of vesicles into the nucleus (Szöllösi and Szöllösi, 1988). Only a fraction of TCA enzymes are involved in the transport process, but MDVs are reported to be selective for their cargo (Shutt and McBride, 2013). Another model involves pyruvate-dependent O-glycosylation of class I enzymes binding to Hsp90 or similar chaperones and then gliding through the nuclear pore (Hardivillé and Hart, 2014). This mechanism does not exclude a role of MDV-like vesicles in the transport process.

Published literature provides precedence for extra-mitochondrial localization of PDH (Chueh et al., 2011; Mitra et al., 2005; Sutendra et al., 2014). Similar to our results in the pre-implantation embryo, all three subunits of PDH can be detected during the S phase of the cell cycle in the nucleus of lung cancer cell lines (Sutendra et al., 2014). Also, this nuclear PDH enzyme complex is active and influences only a subset of histone acetylation patterns (Sutendra et al., 2014). Notable differences include the need for large amounts of growth factors for nuclear PDH to be detected in cancer cell lines and, more importantly, that no TCA cycle enzyme such as citrate synthase and IDH, that were included in the study, were detected in the nucleus. These differences between the embryo and the cancer cell lines will be important in resolving questions regarding metabolic control of normal development and cancer. It will also be very interesting to determine whether the process outlined here for normal development is found either in part or in full in the context of any other cancer or stem cell development. An additional avenue to explore will be to determine whether these observations have clinical relevance in infertility research, including the efficiency of the in vitro fertilization procedures. Infertility is often associated with metabolic disorders and cellular stress signals. Whether some of these dysfunctions result from perturbation of processes described here warrants future analysis.

STAR METHODS

Detailed methods are provided in the online version of this paper and include the following:

- KEY RESOURCES TABLE
- CONTACT FOR REAGENT AND RESOURCE SHARING
- EXPERIMENTAL MODEL AND SUBJECT DETAILS
 - Mouse embryo culture
 - Human embryo culture
- METHOD DETAILS
 - Reagents
 - BrUTP incorporation
 - Immunolocalization in isolated nuclei
 - Antibody staining for immunofluorescence
 - JC1 and Rhod-2A staining
 - Measurement of metabolite levels
 - Enzymatic Analyses in Isolated Nuclei
- QUANTIFICATION AND STATISTICAL ANALYSIS

SUPPLEMENTAL INFORMATION

Supplemental Information includes six figures and can be found with this article online at <http://dx.doi.org/10.1016/j.cell.2016.12.026>.

AUTHOR CONTRIBUTIONS

R.N. and M.S.S. conceived and performed experiments and wrote the initial draft of the manuscript. F.C., D.B., and Y.Z. performed experiments. R.K. and A.T.C. provided reagents and research material. U.B. supervised the project, secured funding, and wrote the manuscript.

ACKNOWLEDGMENTS

We would like to thank Wei Liao for help in bioinformatics analysis of RNA expression, Shubhendu Senroy for setting up the embryo culture system during the early phases of this work, and all members of our laboratory for their suggestions and support. The human embryo studies were approved by the full UCLA Institutional Review Board (IRB#11-002027) and the UCLA Embryonic Stem Cell Research Oversight (ESCRO) Committee (2007-005). We thank Dr. David Jelinek and Dr. Hilary Coller at UCLA for help with the IDH enzyme assay. We thank the UCLA metabolism group including Drs. Lowry, Coller, Plath, Graeber, and Christofk for advice and discussions. We are extremely grateful for the support provided by the NIH Director's Pioneer Award to U.B. (DP1DK098059-04) that enabled this laboratory to initiate research in metabolism and development of mammalian embryos. We would also like to gratefully acknowledge critical research support from the UCLA Broad Stem Cell Research Center and thank Director Owen Witte for his continued support. F.C. is supported by a China Scholarship Council Award and a California Institute for Regenerative Medicine pre-doctoral fellowship.

Received: September 10, 2016

Revised: October 23, 2016

Accepted: December 16, 2016

Published: January 12, 2017

REFERENCES

- Acton, B.M., Jurisicova, A., Jurisica, I., and Casper, R.F. (2004). Alterations in mitochondrial membrane potential during preimplantation stages of mouse and human embryo development. *Mol. Hum. Reprod.* **10**, 23–32.
- Aoki, F., Worrad, D.M., and Schultz, R.M. (1997). Regulation of transcriptional activity during the first and second cell cycles in the preimplantation mouse embryo. *Dev. Biol.* **181**, 296–307.

- Barbehenn, E.K., Wales, R.G., and Lowry, O.H. (1978). Measurement of metabolites in single preimplantation embryos: a new means to study metabolic control in early embryos. *J. Embryol. Exp. Morphol.* 43, 29–46.
- Baumann, C.G., Morris, D.G., Sreenan, J.M., and Leese, H.J. (2007). The quiet embryo hypothesis: Molecular characteristics favoring viability. *Mol. Reprod. Dev.* 74, 1345–1353.
- Biggers, J.D., Whittingham, D.G., and Donahue, R.P. (1967). The pattern of energy metabolism in the mouse oocyte and zygote. *Proc. Natl. Acad. Sci. USA* 58, 560–567.
- Biggers, J.D., Summers, M.C., and McGinnis, L.K. (1997). Polyvinyl alcohol and amino acids as substitutes for bovine serum albumin in culture media for mouse preimplantation embryos. *Hum. Reprod. Update* 3, 125–135.
- Brinster, R.L. (1967a). Oxygen consumption of preimplantation embryos. *Exp. Cell Res.* 47, 337–344.
- Brinster, R.L. (1967b). Carbon dioxide production from glucose by the preimplantation mouse embryo. *Exp. Cell Res.* 47, 271–277.
- Brinster, R.L. (1969). Incorporation of carbon from glucose and pyruvate into the preimplantation mouse embryo. *Exp. Cell Res.* 58, 153–158.
- Brown, J.J., and Whittingham, D.G. (1991). The roles of pyruvate, lactate and glucose during preimplantation development of embryos from F1 hybrid mice in vitro. *Development* 112, 99–105.
- Calarco, P.G., and Brown, E.H. (1969). An ultrastructural and cytological study of preimplantation development of the mouse. *J. Exp. Zool.* 171, 253–283.
- Chueh, F.Y., Leong, K.F., Cronk, R.J., Venkitachalam, S., Pabich, S., and Yu, C.L. (2011). Nuclear localization of pyruvate dehydrogenase complex-E2 (PDC-E2), a mitochondrial enzyme, and its role in signal transducer and activator of transcription 5 (STAT5)-dependent gene transcription. *Cell. Signal.* 23, 1170–1178.
- Cockburn, K., and Rossant, J. (2010). Making the blastocyst: Lessons from the mouse. *J. Clin. Invest.* 120, 995–1003.
- Dikov, A., Dimitrova, M., Krieg, R., and Halbhuber, K.J. (2004). New fluorescent method for the histochemical detection of tripeptidyl peptidase I using glycyl-L-prolyl-L-met-2-anthraquinonyl hydrazide as substrate. *Cell. Mol. Biol.*, 50 *Online Pub.* OL565–568.
- Donohoe, D.R., and Bultman, S.J. (2012). Metabolopigenetics: Interrelationships between energy metabolism and epigenetic control of gene expression. *J. Cell. Physiol.* 227, 3169–3177.
- Duverger, E., Roche, A.C., and Monsigny, M. (1996). N-acetylglucosamine-dependent nuclear import of neoglycoproteins. *Glycobiology* 6, 381–386.
- Egloff, S., and Murphy, S. (2008). Cracking the RNA polymerase II CTD code. *Trends Genet.* 24, 280–288.
- Guinez, C., Morelle, W., Michalski, J.C., and Lefebvre, T. (2005). O-GlcNAc glycosylation: A signal for the nuclear transport of cytosolic proteins? *Int. J. Biochem. Cell Biol.* 37, 765–774.
- Hardivillé, S., and Hart, G.W. (2014). Nutrient regulation of signaling, transcription, and cell physiology by O-GlcNAcylation. *Cell Metab.* 20, 208–213.
- Holness, M.J., and Sugden, M.C. (2003). Regulation of pyruvate dehydrogenase complex activity by reversible phosphorylation. *Biochem. Soc. Trans.* 31, 1143–1151.
- Houghton, F.D., Thompson, J.G., Kennedy, C.J., and Leese, H.J. (1996). Oxygen consumption and energy metabolism of the early mouse embryo. *Mol. Reprod. Dev.* 44, 476–485.
- Lane, M., and Gardner, D.K. (2000). Lactate regulates pyruvate uptake and metabolism in the preimplantation mouse embryo. *Biol. Reprod.* 62, 16–22.
- Lange, A., Mills, R.E., Lange, C.J., Stewart, M., Devine, S.E., and Corbett, A.H. (2007). Classical nuclear localization signals: Definition, function, and interaction with importin alpha. *J. Biol. Chem.* 282, 5101–5105.
- Lawitts, J.A., and Biggers, J.D. (1991). Optimization of mouse embryo culture media using simplex methods. *J. Reprod. Fertil.* 91, 543–556.
- Leese, H.J. (2012). Metabolism of the preimplantation embryo: 40 years on. *Reproduction* 143, 417–427.
- Leese, H.J., and Barton, A.M. (1984). Pyruvate and glucose uptake by mouse ova and preimplantation embryos. *J. Reprod. Fertil.* 72, 9–13.
- Li, L., Zheng, P., and Dean, J. (2010). Maternal control of early mouse development. *Development* 137, 859–870.
- Martinez-Pastor, B., Cosentino, C., and Mostoslavsky, R. (2013). A tale of metabolites: The cross-talk between chromatin and energy metabolism. *Cancer Discov.* 3, 497–501.
- McLaren, A., and Biggers, J.D. (1958). Successful development and birth of mice cultivated in vitro as early as early embryos. *Nature* 182, 877–878.
- Mitra, K., Rangaraj, N., and Shivaji, S. (2005). Novelty of the pyruvate metabolic enzyme dihydrolipopamide dehydrogenase in spermatozoa: Correlation of its localization, tyrosine phosphorylation, and activity during sperm capacitation. *J. Biol. Chem.* 280, 25743–25753.
- Niakan, K.K., and Eggan, K. (2013). Analysis of human embryos from zygote to blastocyst reveals distinct gene expression patterns relative to the mouse. *Dev. Biol.* 375, 54–64.
- Quinn, P., and Wales, R.G. (1974). Fixation of carbon dioxide by preimplantation rabbit embryos in vitro. *J. Reprod. Fertil.* 36, 29–39.
- Schultz, R.M. (1993). Regulation of zygotic gene activation in the mouse. *Bioessays* 15, 531–538.
- Shutt, T.E., and McBride, H.M. (2013). Staying cool in difficult times: Mitochondrial dynamics, quality control and the stress response. *Biochim. Biophys. Acta* 1833, 417–424.
- Sies, H., Graf, P., and Crane, D. (1983). Decreased flux through pyruvate dehydrogenase during calcium ion movements induced by vasopressin, alpha-adrenergic agonists and the ionophore A23187 in perfused rat liver. *Biochem. J.* 212, 271–278.
- Sugiura, A., McLelland, G.L., Fon, E.A., and McBride, H.M. (2014). A new pathway for mitochondrial quality control: Mitochondrial-derived vesicles. *EMBO J.* 33, 2142–2156.
- Sutendra, G., Kinnaird, A., Dromparis, P., Paulin, R., Stenson, T.H., Haromy, A., Hashimoto, K., Zhang, N., Flaim, E., and Michelakis, E.D. (2014). A nuclear pyruvate dehydrogenase complex is important for the generation of acetyl-CoA and histone acetylation. *Cell* 158, 84–97.
- Szöllösi, M.S., and Szöllösi, D. (1988). ‘Blebbing’ of the nuclear envelope of mouse zygotes, early embryos and hybrid cells. *J. Cell Sci.* 91, 257–267.
- Tomilov, A., Bettaieb, A., Kim, K., Sahdeo, S., Tomilova, N., Lam, A., Hagopian, K., Connell, M., Fong, J., Rowland, D., et al. (2014). Shc depletion stimulates brown fat activity in vivo and in vitro. *Aging Cell* 13, 1049–1058.
- Trimarchi, J.R., Liu, L., Porterfield, D.M., Smith, P.J., and Keefe, D.L. (2000). Oxidative phosphorylation-dependent and -independent oxygen consumption by individual preimplantation mouse embryos. *Biol. Reprod.* 62, 1866–1874.
- Weaver, J.R., Susiarjo, M., and Bartolomei, M.S. (2009). Imprinting and epigenetic changes in the early embryo. *Mamm. Genome* 20, 532–543.
- Williams, E.G., Wu, Y., Jha, P., Dubuis, S., Blattmann, P., Argmann, C.A., Houten, S.M., Amariuta, T., Wolski, W., Zamboni, N., et al. (2016). Systems proteomics of liver mitochondria function. *Science* 352, aad0189.
- Williamson, J.R., Walajtys-Rode, E., and Coll, K.E. (1979). Effects of branched chain alpha-ketoacids on the metabolism of isolated rat liver cells. I. Regulation of branched chain alpha-ketoacid metabolism. *J. Biol. Chem.* 254, 11511–11520.
- Xiao, M., Yang, H., Xu, W., Ma, S., Lin, H., Zhu, H., Liu, L., Liu, Y., Yang, C., Xu, Y., et al. (2012). Inhibition of α -KG-dependent histone and DNA demethylases by fumarate and succinate that are accumulated in mutations of FH and SDH tumor suppressors. *Genes Dev.* 26, 1326–1338.
- Xue, Z., Huang, K., Cai, C., Cai, L., Jiang, C.Y., Feng, Y., Liu, Z., Zeng, Q., Cheng, L., Sun, Y.E., et al. (2013). Genetic programs in human and mouse early embryos revealed by single-cell RNA sequencing. *Nature* 500, 593–597.

STAR★METHODS

KEY RESOURCES TABLE

REAGENT or RESOURCE	SOURCE	IDENTIFIER
Antibodies		
Mouse anti-PCNA	Abcam	Cat#ab29
Rabbit anti-phosphohistone 3	Abcam	Cat#ab47297
Rat anti-tubulin	Abcam	Cat#ab6160
Mouse anti-Pol II	Santa Cruz	Cat#8WG16
Rabbit anti-Sirt1	Abcam	Cat#ab7343
Mouse anti-O-linked glycosylation antibody (RL2)	Abcam	Cat#ab2739
Rabbit anti-H3K4 acetylation	Abcam	Cat#ab113672
Rabbit anti-H3K27 acetylation	Abcam	Cat#ab45173
Mouse anti-H3K9 acetylation	Abcam	Cat#ab12179
Mouse anti-H3K4 tri-methylation	Abcam	Cat#ab12209
Rabbit anti-phospho-PDH	Abcam	Cat#ab92696
Mouse anti-PDH	Abcam	Cat#ab110334
Mouse anti-PDH	Santa Cruz	Cat#sc-377092
Rabbit anti-PDK1 antibody	Abcam	Cat#ab52893
Goat anti-PDP1 antibody	Santa Cruz	Cat#sc87354
Mouse anti-PCB antibody	Abcam	Cat#ab110314
Rabbit anti-CS antibody	Abcam	Cat#ab96600
Mouse aconitase 2 antibody	Abcam	Cat#ab110321
Rabbit anti-IDH3A antibody	Abcam	Cat#ab58641
Goat anti-KGDH antibody	Santa Cruz	Cat#sc-48589
Rabbit anti-SCS antibody	Cell Signaling	Cat#8071
Mouse anti-SDH antibody	Abcam	Cat#ab14715
Mouse anti-MDH2 antibody	Abcam	Cat#ab92867
Mouse anti-HSP70 antibody	Santa Cruz	Cat#sc24
Mouse anti-HSP90 antibody	Abcam	Cat#ab13492
Mouse anti-H3K9me3 antibody	Abcam	Cat#ab8898
Rabbit anti-H3K14 acetylation antibody	Epigenetik	Cat#A4032
Mouse anti-Sp1 antibody	Abcam	Cat#ab77441
Rabbit anti-myc antibody	Santa Cruz	Cat#sc40
Chemicals, Peptides, and Recombinant Proteins		
ST045849	Timtec	ST045849
17-Demethoxy-17-(2-propenylamino)geldanamycin (17-AAG)	Torcris Biosciences	1515
JC1	Thermofisher	T3168
Rhod-2AM	Thermofisher	R1244
5-Cyano-2,3-di-(p-tolyl)tetrazolium chloride	Polysciences	19292
Pyruvic Acid, sodium salt 1- ¹⁴ C	Perkin Elmer	NEC255050UC
Critical Commercial Assays		
NAD ⁺ /NADH measurement	Promega	Cat#G9071
GSH/GSSG measurement	Promega	Cat#V6611
ATP measurement	Promega	Cat#FF2000
ADP measurement	Promega	Cat#V6930

(Continued on next page)

Continued

REAGENT or RESOURCE	SOURCE	IDENTIFIER
EU Click-iT RNA imaging kit	Thermofisher	Cat#C10330
Experimental Models: Organisms/Strains		
Mouse: B6C3F1/J	The Jackson Laboratory	Stock No: 100010
Experimental Models: Cell Lines		
Mouse: embryo culture	This lab	N/A
Human: embryo culture	This lab	N/A
Software and Algorithms		
Graphpad Prism 7	GraphPad Software Inc	http://www.graphpad.com/
TraceFinder 3.3	Thermofisher	https://www.thermofisher.com/order/catalog/product/OPTON-30491

CONTACT FOR REAGENT AND RESOURCE SHARING

Further information and requests for resources and reagents should be directed to and will be fulfilled by the Lead Contact Utpal Banerjee (banerjee@mbi.ucla.edu).

EXPERIMENTAL MODEL AND SUBJECT DETAILS**Mouse embryo culture**

All animal care and procedures used in this study are approved by the Animal Regulatory Committee (ARC) of the University of California at Los Angeles (UCLA).

Mouse zygotes and pre-implantation embryos were collected from super-ovulated 4-week old C57BL/6J X C3He (Jackson labs) F1 females. Mice were super-ovulated by peritoneal injection of 7.5 IU of PMSG (Pregnant Mare Serum Gonadotropin) to stimulate egg production, followed by 7.5 IU of hCG (human Chorionic Gonadotropin) 48hrs after PMSG. Embryos were obtained by mating the super-ovulated females with C57BL/6 X C3He F1 males. Mating was confirmed by the presence of vaginal plug. For isolation of fertilized 1-cell zygotes, super-ovulated females were euthanized 18hrs post-hCG and zygotes were dissected out of the ampulla in the oviduct. The embryo-cumulus complexes were treated with 300 µg/ml of hyaluronidase to disperse the cumulus cells, washed in mKSOM medium without pyruvate and transferred to the appropriate culture medium (+P or -P) and cultured at 37°C in 5% CO₂. For embryo isolation at later stages, the embryos were flushed from the oviduct at the appropriate times, washed in mKSOM medium and either cultured or fixed immediately for immuno-fluorescence analysis. All mouse embryos used in this study were cultured in a modified KSOM medium whose composition is identical to KSOM in salts, glucose, lactate and pyruvate (95mM NaCl, 2.5mM KCl, 0.35mM KH₂PO₄, 0.20mM MgSO₄, 25mM NaHCO₃, 1.71mM CaCl₂, 0.01 mM EDTA, 0.20mM glucose, 10mM lactate, 0.20mM pyruvate) but was devoid of all amino acids and BSA. The osmolarity of the medium was maintained using 0.1% PVA (poly vinyl alcohol) (Biggers et al., 1997).

Human embryo culture

The human embryo studies were approved by the full UCLA Institutional Review Board (IRB#11-002027) and the UCLA Embryonic Stem Cell Research Oversight (ESCRO) Committee (2007-005). Human pre-implantation embryos for this project were received cryopreserved from an IVF clinic following consent. A total of 10 2PN embryos from 2 donors were used for this project. Human embryos were slow thawed using Thaw-Kit 1 (Vitrolife) according to the manufacturer's protocol. The embryos were cultured in drops of Continuous Single Culture media (Irvine Scientific) supplemented with 20% Quinn's Advantage SPS Serum Protein Substitute (Sage Media) for 0 to 4 sequential days at 37°C, 6% CO₂ and 5% O₂. At varying stages of development from 2PN to compacting morula, the zona pellucida was removed with Tyrode's Acidified Solution (Irvine Scientific) and fixed in 4% paraformaldehyde for 30 min and stained with antibodies as in the previous protocol.

METHOD DETAILS**Reagents**

The following antibodies and drugs were used in this study. Mouse monoclonal antibody against BrdU (Invitrogen B35128) at 1:250 dilution, Mouse anti-PCNA antibody (Abcam ab29) at 1:200 dilution, rabbit anti-Phospho-histone 3 antibody (Abcam ab47297) 1:200 dilution, Rat anti-tubulin antibody (Abcam ab6160) 1:500 dilution, monoclonal antibodies against Pol II CTD phospho S2 (H5) and phospho S5 (H14) from Covance used at 1:50 dilution, mouse, anti-Pol II antibody (8WG16 from Santa Cruz), Rabbit anti-SIRT1 antibody (Abcam ab7343) 1:100 dilution, mouse, anti-O-linked N-acetylglucosamine antibody RL2 (Abcam ab2739) 1:200 dilution, rabbit

anti-H3K4 acetylation (Abcam ab113672) 1:200, rabbit anti-H3K27 acetylation (Abcam ab45173) 1:200, mouse anti-H3K9 acetylation (Abcam ab12179) 1:200, mouse anti-H3K4 tri-methylation (Abcam ab12209) 1:200, rabbit phospho-PDH antibody (abcam ab92696) 1:50, mouse anti-PDH antibody (abcam ab110334) 1:100, mouse anti-PDH antibody (Santa Cruz sc-377092) 1:50, rabbit anti-PDK1 antibody (Abcam ab52893) 1:100, goat anti-PDP1 antibody (Santa Cruz sc87354) 1:100, mouse anti-PCB antibody (Abcam ab110314) 1:200, rabbit anti-CS antibody (Abcam ab96600) 1:500, mouse anti-aconitase-2 antibody (Abcam ab110321) 1:100, rabbit anti-IDH3A antibody (Abcam ab58641) 1:100, goat anti-KGDH antibody (Santa Cruz sc-48589) 1:50, rabbit anti-SCS antibody (Cell Signaling 8071) 1:100, mouse anti-SDHA antibody (Abcam ab14715) 1:100, mouse anti-MDH-2 antibody (Abcam ab92867) 1:100, mouse HSP70 antibody (Santa Cruz sc24) 1:50, mouse anti HSP90 antibody (Abcam ab13492) 1:100, mouse H3K9me3 antibody (Abcam ab8898) 1:200, rabbit anti-H3K14 acetylation antibody (Epigenetik A4032) 1:200, mouse anti-SP1 antibody (Abcam ab77441) 1:100, rabbit anti-Myc antibody (Santa Cruz sc40) 1:50. STO45849 was purchased from TimTec, HSP90 inhibitor, 17-AAG (17-Demethoxy-17-(2-propenylamino)geldanamycin) was purchased from Torcis biosciences. JC1 and rhod-2AM dyes were purchased from Invitrogen.

BrUTP incorporation

BrUTP incorporation was performed using the protocol described by Aoki et al., 1997. BrUTP incorporation was also performed using the Click-iT RNA imaging kit from Invitrogen (cat no. C10330). Live embryos were incubated in 5-ethynyl uridine (EU) for 30mins for incorporation into nascent transcripts, following which they were fixed in 4% paraformaldehyde for 30mins at room temperature and permeabilized in PBST for 20mins. Click-iT cocktail was freshly prepared and the embryos were incubated in it for 30mins at room temperature protected from light. The embryos were subsequently washed in Click-iT reaction rinse buffer and incubated in To-Pro in PBS to mark the nuclei and mounted in Vectashield medium for microscopy.

Immunolocalization in isolated nuclei

Staining nuclei devoid of the surrounding cytoplasm followed the methods developed by Coonen et al., 1994. Embryos are removed from the mKSOM medium, washed several times with PBS, transferred with minimal amounts of PBS to a microdrop of 0.01N HCl / 0.1% Tween20 in distilled sterile water on a glass slide. Within a few minutes the Zona and the cytoplasm begin to disintegrate and the nucleus becomes clearly visible and following removal of all the cytoplasm, the nuclei remain attached to the glass slide. The slides are washed with several rounds of PBS to remove the remaining cytoplasm. The attached nuclei are fixed with 4% paraformaldehyde, washed in PBST, and stained with specific antibodies.

Antibody staining for immunofluorescence

Staged embryos are fixed in 4% paraformaldehyde for 30 min at room temperature, permeabilized for 30mins in PBS with 0.4% Triton (PBST), blocked in PBST with 3% albumin for 30mins and incubated with the desired primary antibody in PBST plus 3% albumin (PBSTA) overnight at 4°C. The following day the embryos were washed in PBST four times for 10min each, blocked with PBSTA, incubated with the appropriate secondary antibody (1/300 dilution) overnight at 4°C. Embryos were washed again 3 times for 10min each in PBST. Nuclei were counterstained with To-Pro for 10mins, washed once again in PBST for 10mins, deposited on glass slides and mounted in Vecta-shield (Vector Laboratories) medium. Images were captured using a Zeiss LSM 700 confocal microscope. Data were quantified using the Prism software package, using a two-tailed unpaired t test. The numbers of embryos used for each experiment are reported in the Figure legend. Data are considered significant if $p < 0.05$, and the error bars are \pm SEM.

JC1 and Rhod-2A staining

Live 2-cell embryos were incubated in mKSOM containing 0.1 μ g/ml of JC1 (Life Technologies) or 5 μ M Rhod-2AM (Life Technologies) for 30 min in 5% CO₂ at 37°C. After incubation, embryos were washed several times in mKSOM, transferred to depression slides and mounted in the medium.

Measurement of metabolite levels

ATP was measured using the ENLIGHTEN ATP assay system according to the manufacturer's instructions (Promega, WI, USA). Briefly, ATP was extracted from embryos using 2.5% TCA and neutralized with 0.1 M Tris-acetate buffer pH 7.75. Following addition of an equal volume of rL/L Reagent (Promega), luminescence was measured as readout for ATP levels. ADP was measured using the ADP-glo detection kit (Promega, WI, USA). Reduced glutathione levels were determined using the GSH-Glo bioluminescent assay (Promega, WI, USA). Embryos (in 10 μ L mKSOM) were snap frozen in liquid nitrogen. The thawed samples were added directly to 2X GSH-Glo reagent containing a modified luciferin and glutathione transferase, and incubated in the dark for 30 min at room temperature. An equal volume of luciferin detection reagent was added and the luminescence detected after 15 min. NAD⁺ and NADH levels were determined using the NAD⁺/NADH Glo cycling assay, according to the manufacturer's instructions (Promega, WI, USA). Briefly, both NAD⁺ and NADH were extracted from the embryos in a carbonate buffered base solution containing 1% DTAB, 10 mM nicotinamide, 0.05% Triton X-100, pH 10.7. The embryos were freeze-thawed in liquid nitrogen and centrifuged through a filter with a 10kDa mW cut-off. Samples for NAD⁺ determination were neutralized with 0.4 N HCl. Both NAD⁺ and NADH samples were heated for 20 min at 60°C. The assay reagent was added to the samples, which were then incubated for 3 hr for cycling, after which the luminescence was determined.

The assay to measure the response of the TCA cycle metabolites to starvation and re-feeding was adapted from the approach of Lowry. For each condition, approximately 250 embryos were cultured in +P media until 48 hr post-hCG. Each condition was assayed in triplicate, with each replicate containing approximately 250 embryos, the exact number of which was used to normalize the data. For the fully fed condition, embryos were washed twice in a large volume of fresh +P media, but which lacked lactate and glucose, and incubated for 30 min. Following which, the embryos were incubated for a further 20 min in fresh +P media (lacking lactate and glucose but containing pyruvate) and then the metabolites were extracted using cold 80% methanol. For the starved condition, embryos were washed twice in starvation media (lacking pyruvate, lactate and glucose), incubated for 30 min, following which the embryos were washed with fresh starvation medium and the metabolites isolated. For the re-fed condition, following a 30 min starvation, embryos were incubated with +P media (containing pyruvate, but not lactate or glucose) for 20 min. The embryos were washed twice in fresh +P media (containing pyruvate, but not lactate or glucose) and the metabolites extracted using cold 80% methanol. For samples analyzed under steady state conditions (Figure 5J), embryos were transferred into 80% methanol in 5 µl of +P or -P media, which contained 10 mM lactate. The lactate level in the media is in excess and therefore insensitive to culture conditions. In Figure 5J, the lactate level was used as an internal control (this was not possible in 5H,I since lactate was omitted from the media). Dried metabolites were re-suspended in 15 µl 50% ACN and 10 µl were injected for chromatographic separation using the Thermo Scientific Ion Chromatography System (ICS) 5000 coupled to a Thermo Scientific Q Exactive run in negative polarity mode. The gradient ran from 10 mM to 90 mM KOH over 25 min with a flow rate of 350 µl / min. The settings for the HESI-II source were: S-lens 50, Sheath Gas 18, Aux Gas 4, spray heater 320°C, and spray voltage -3.2 kV. Metabolites were identified based on accurate mass (± 3 ppm) and retention times of pure standards. Relative amounts of metabolites were quantified using TraceFinder 3.3. Oxaloacetate and isocitrate could not be measured accurately using this approach with tractable numbers of embryos. The data were analyzed using the Prism software package. The difference between metabolites in each condition was compared using unpaired two-tailed Student's t tests.

Enzymatic Analyses in Isolated Nuclei

Nuclei were isolated from two-cell embryos as described above. PDH activity was measured by adopting a method described by Lane and Gardner to measure pyruvate oxidation in live embryos (Lane and Gardner, 2000). In these experiments pyruvate dehydrogenase activity was measured by incubating 200 isolated nuclei with assay solution (50 mM MOPS pH 7.4, 0.2 mM MgCl₂, 0.01 mM CaCl₂, 0.3 mM thiamine pyrophosphate, 0.12 mM coenzyme A, 2 mM NAD⁺, 2.64 mM L-cysteine HCl) containing [1-¹⁴C] pyruvate 0.085 mCi/ml. Each condition was performed in triplicate (and each replicate contained 200 nuclei). The nuclei were attached to pre-cut coverslips that were fixed in the lid of a microcentrifuge vial and a 3 µL drop of assay medium was placed on the nuclei. The vial lid was placed on a vial containing 1.65 mL of 25 mM NaHCO₃ pre-gassed with 5% CO₂ in air, which trapped labeled CO₂ generated from pyruvate. Samples were incubated for 5 hr at 37°C. Controls included a 3 µL drop of assay medium on the lid without nuclei in order to control for spontaneous breakdown of the label. Total counts were determined by the addition of a 3 µL drop of medium straight into the 1.65 mL NaHCO₃. After 5 hr the vials were opened, and 1 mL of the NaHCO₃ removed and placed into a scintillation vial containing 200 µL of 0.1 M NaOH. Vials were sealed and stored overnight. The following morning, 10 mL of scintillation fluid was added to each vial. The vials were vortexed and counted for 4 min each, and the results were normalized against the total number of counts in the assay medium. Quantification was performed using an unpaired two-tailed Student's t test.

IDH3 assay

Nuclei were isolated from embryos cultured either in +P or -P medium on a glass slide were washed in PBS twice and IDH3 activity was determined in situ using an enzymatic assay. The assay buffer (Tris pH 7.4 (50mM), Mg₂SO₄ (1mM), NAD⁺ (1mM), isocitrate (10mM), Cynoditolyl Tetrazolium (500 µg/ml) (Polysciences 19292-100) and PMS (25 µg/ml)). For negative controls, isocitrate was eliminated from the assay buffer. The nuclei were incubated for 4 hr, washed in PBS several times and mounted on Vectashield medium and the images were collected using confocal microscope.

QUANTIFICATION AND STATISTICAL ANALYSIS

Statistical parameters are reported in the figures and figure legends. Data is considered significant if p < 0.05 (see [Method Details](#)). Statistical analysis was performed using the Graphpad Prism 7 software.

Supplemental Figures

Cell

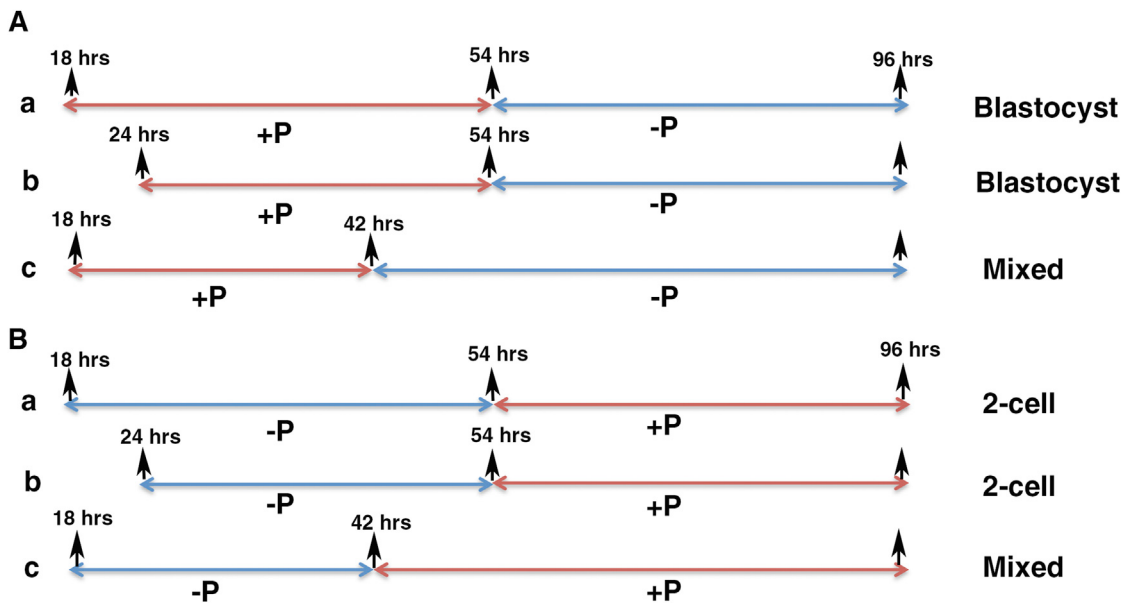


Figure S1. Defining the Critical Period for Pyruvate Requirement, Related to Figure 1

The 30hr critical time window for pyruvate requirement is shown in Figures 1J and 1K. This interval was determined by transferring embryos from +P to -P culture media (A) and vice versa (B), at the indicated times, shown in this figure.

The following was the distribution of embryos at different stages, for each experiment between 70-80 embryos were used and were cultured for 96 hr.

(A) (a) For the 18-54 hr +P to -P experiment, 70 embryos developed to the blastocysts, 3 were blocked at the 2-cell stage. (b) For the 24-54hrs +P to -P experiment, 72 embryos developed to the blastocyst stage, 6 were arrested at the 1-cell stage and 1- embryo at the 2-cell stage. (c) For the 18-42 hr +P to -P experiment, 26 embryos were blocked at the 2-cell stage and 44 embryos developed to blastocysts.

(B) (a) 18-54hrs -P to +P experiment, 48 were blocked at 2-cell stage, 14 embryos were blocked at 1-cell stage and 3 embryos at 3-cell stage. (b) For 24-54 hr -P to +P experiment, 54 were blocked at 2-cell stage, 11 embryos were blocked at the 1-cell stage and 6 embryos at the 3-cell stage. (c) for the 18-42hrs -P to +P experiment, 36 embryos were blocked at the 2-cell stage and 44 embryos eventually developed to the blastocysts.

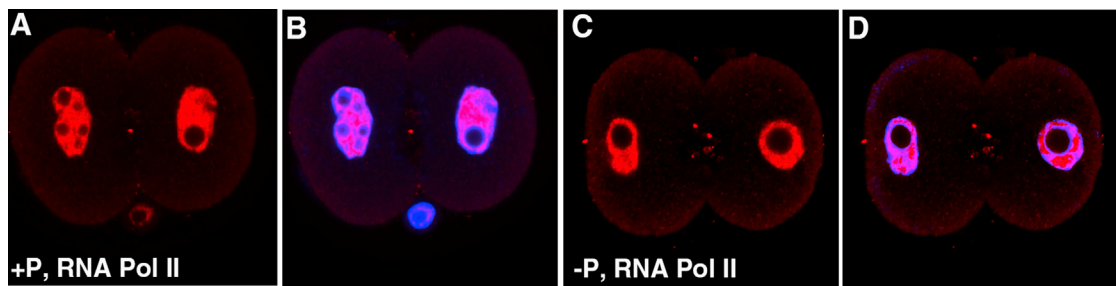


Figure S2. Role of Pyruvate in ZGA, Related to Figure 2

Total RNA Pol II in the nucleus (A–D) is not dependent on exogenously provided pyruvate (Compare with Figures 2C–2F and 2I–2N).

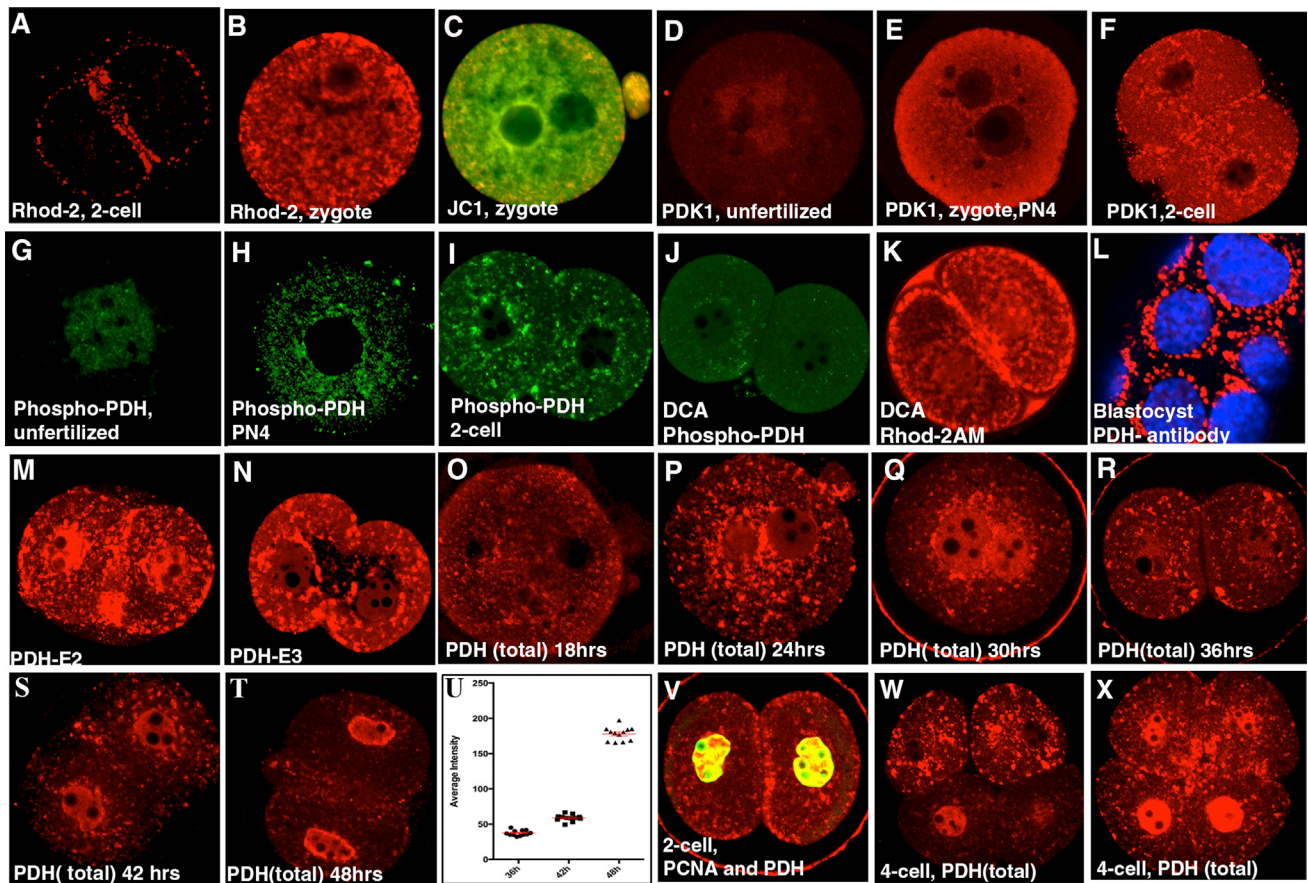


Figure S3. Mitochondrial Activity and Developmental Regulation of PDK and PDH, Related to Figure 3

(A) 2-cell embryo cultured in +P medium stained for Rhod-2AM shows only a small number mitochondria near the plasma membrane have increased levels of Ca^{2+} , hence higher in activity than the ones deeper inside the embryo.

(B) In contrast, in an earlier pro-nuclear stage zygote (PN2), Rhod-2 staining extends to mitochondria throughout the zygote.

(C) JC1 staining of a zygote at PN3 stage (compare with 2-cell stage, [Figure 3B](#)).

(D-F) PDK1 expression and localization.

PDK1 expression is marginally detectable in unfertilized oocytes (D), becomes more prominent in PN4 zygotes (E) and is prominently mitochondrial at the 2-cell stage (F) At all stages, PDK1 is excluded from the nucleus.

(G-I) Phospho-PDH (inactive) closely parallels PDK1 expression.

p-PDH is first detected in the unfertilized oocyte (G), upregulated in the one cell (PN4) embryo (H), and seen at high levels in the mitochondrion of 2-cell embryos (I). At no stage of development is inactive PDH detected in the nucleus.

(J and K) DCA (Dichloroacetate), a PDK inhibitor causes significant reduction in p-PDH staining in the mitochondria (J) and an increase in Rhod-2AM staining (K).

(L) α -PDH antibody (ab110334) that does not recognize the inactive form of PDH, and is nuclear at the 2-cell stage ([Figure 3H](#)), is nevertheless, mitochondrial at the later, blastocyst stage. Nuclei are marked with To-Pro.

(M and N) PDH-E2 (M) and PDH-E3 (N), the two subunits of PDH other than the PDH-E1 subunit (shown in [Figures 3E](#) and [3H](#)) are also detected in the nucleus. (O-U) Developmental profile of PDH^{total} expression. (O) at 18 hr post-hCG PDH expression is exclusively mitochondrial with no visible nuclear staining. (P) at 24 hr post-hCG (PN3), low levels of PDH is visible in the nucleus, but majority of the staining is still in the mitochondria. (Q) at 30 hr post-hCG (PN5) strong nuclear staining is visible with a concomitant decrease of the staining in the mitochondria. (R) 36 hr post-hCG, a just formed 2-cell shows high levels of PDH staining in the mitochondria with very low levels in the nucleus. (S) at 42 hr post-hCG, PDH staining is observed both in the mitochondria and the nucleus. (T) 48 hr post-hCG, PDH staining is high in the nucleus with reduced levels in the mitochondria. (U) Quantitation of the nuclear signal of PDH from 2-cell embryos at 36 (n = 12), 42(n = 8), 48 hr (n = 12) respectively.

(V) 42 hr post-hCG, the 2-cell embryos are in S-phase of cell cycle. PDH staining (red) colocalizes with PCNA (green, S-phase marker) in the nucleus.

(W and X) 4-cell embryos from in vivo collection often show two sister cells with exclusively mitochondrial PDH while the two sister cells, slightly asynchronous with the first pair show significant nuclear staining (W). In other 4-cell embryo example (X) from the same collection, all four cells show dual nuclear and mitochondrial localization of PDH. Data is presented as the means \pm SEM.

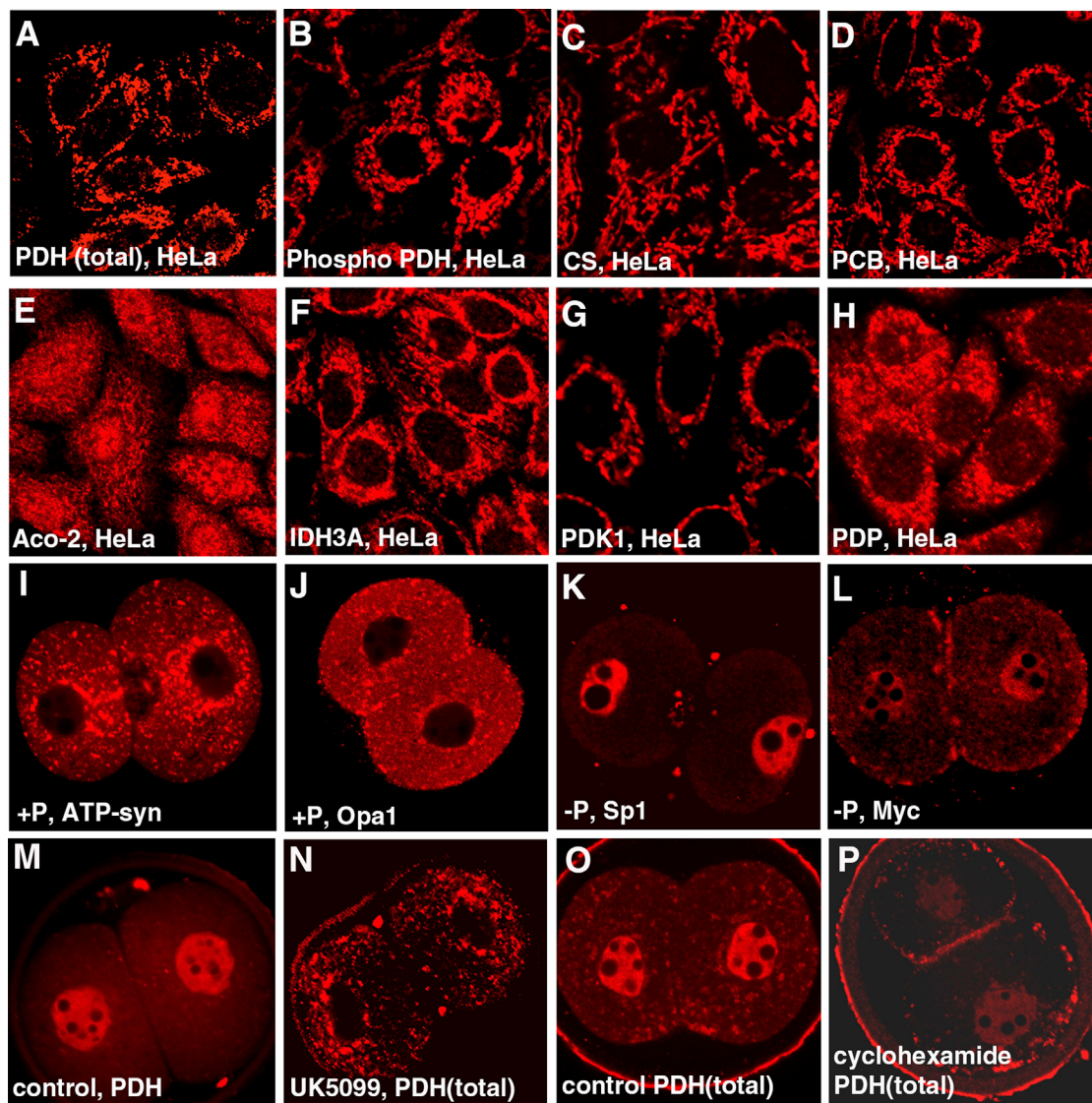


Figure S4. Staining Controls for Figure 4, Related to Figure 4

(A–H) Localization of PDH, PCB and TCA cycle proteins in HeLa cells. Confluent HeLa cells were stained for PDH^{total} (A) PDH^{inactive} (B), CS (C), PCB (D), Aco-2 (E), IDH3A (F), PDK1 (G) and PDP (H). With the exception of Aco-2, all other TCA enzymes and associated proteins are exclusively localized to the mitochondria and not detected in the nucleus.

(I–J) Canonical mitochondrial proteins ATP-syn (I) and Opa1 (J) are not detected in the nucleus after culture to 54hrs post-hCG.

(K–L) Canonical nuclear proteins, Sp1 (K) and Myc (L) do not lose their nuclear localization when cultured in a -P medium until 54hrs post-hCG.

(M and N) A block in the pyruvate import to the mitochondria by UK5099 which targets specifically mitochondrial pyruvate import blocks nuclear translocation of PDH (N).

(O and P) Blocking protein translation using Cyclohexamide treatment of embryos reduces the level of total PDH in the cell but nuclear PDH is observed under these conditions (P).

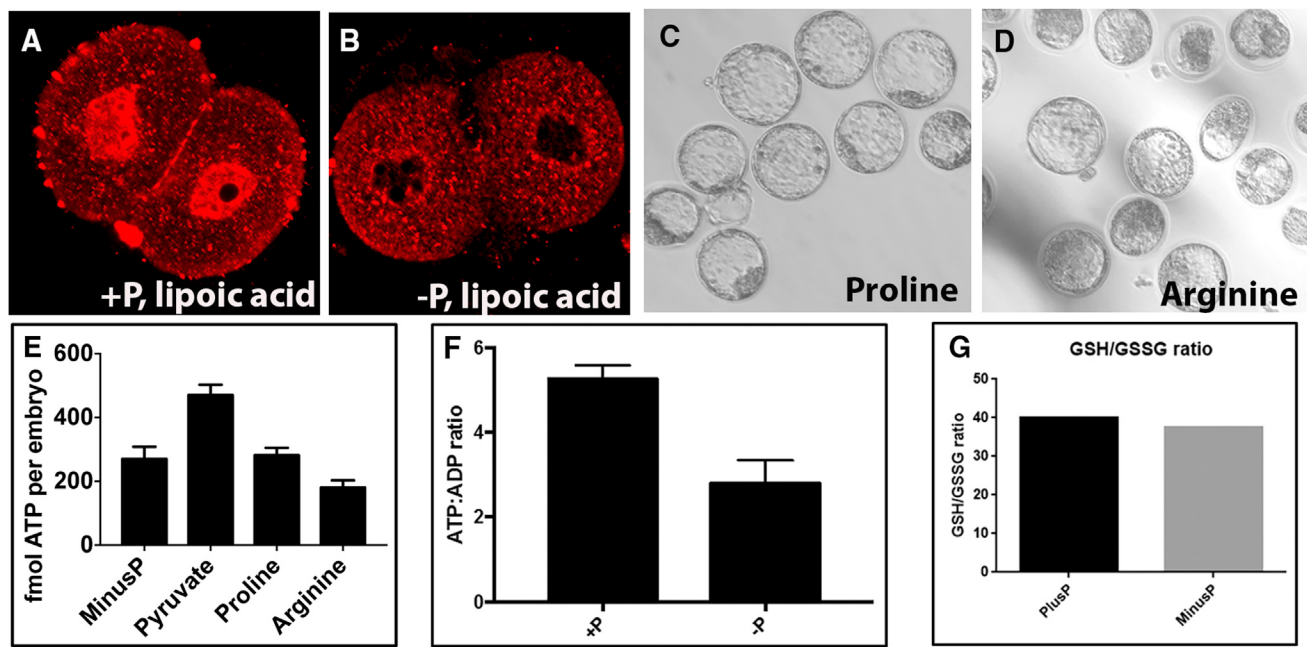


Figure S5. Nuclear Localization and Rescue Experiments, Related to Figure 5

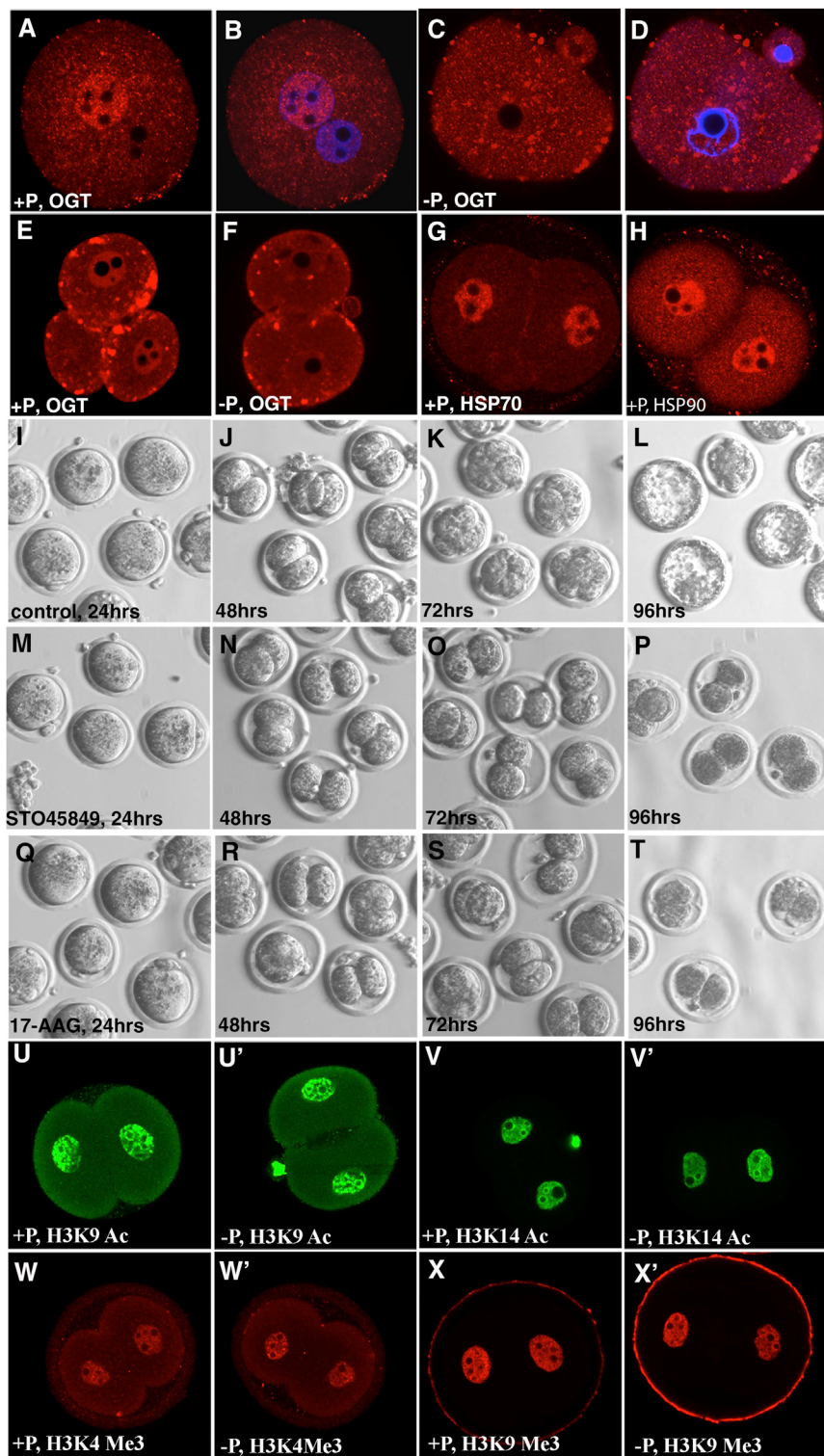
(A and B) Localization of proteins containing a conjugated lipoic acid moiety (A) embryos cultured +P media, (B) embryos in -P media.

(C and D) Representative images of embryos cultured from the zygote stage to the blastocyst in medium containing 1 mM proline or 1 mM arginine.

(E) The ATP levels relative to +P embryos, in two-cell embryos cultured in -P medium or -P medium supplemented with 1 mM proline or 1 mM arginine, respectively. ATP levels are significantly lower in -P, proline and arginine cultured embryos compared to control ($p = 0.0343$, $p = 0.0005$, $p < 0.0001$, respectively, $n = 6$).

(F) The ATP/ADP ratio in embryos cultured in +P and -P media. The ATP/ADP ratio is significantly lower in -P media ($p = 0.0002$, $n = 4$).

(G) The GSH/GSSG ratio in embryos cultured in +P and -P media. The ratio is not significantly different in +P or -P media ($n = 4$). Data is presented as the means \pm SEM.

**Figure S6. O-glycosylation and Pyruvate-Dependent Nuclear Transport, Related to Figure 6**

(A–F) Subcellular localization of OGT in +P and –P medium. OGT is localized to the male pro-nucleus and in the cytoplasm in PN4 zygotes cultured in +P medium (A, B). In –P medium the nuclear localization to the male pro-nucleus is lost (C, D). In the 2-cell stage, OGT is localized to the nucleus and the cytoplasm (E) and its nuclear localization is lost in embryos cultured in –P medium (F).

(G and H) HSP70 (G) and HSP90 (H) are expressed at high levels in 2-cell embryos.

(legend continued on next page)

(I-L) Control embryos at different stages of developmental progression.

(M-T) Drug induced blockage of OGT by 1 μ M STO45849 (M-P,) and HSP90 function by 10 μ M 17-AAG (Q-T), results in 2-cell block. (Compare M-T with control I-L).

(U-X') Acetylation levels of histone H3K9 and H3K14 (U-V') and trimethylation levels of H3K4 and H3K8 (W-X') are not dependent on exogenously provided pyruvate.